Full Scale Testing of Timber-Concrete Composite Floor Systems

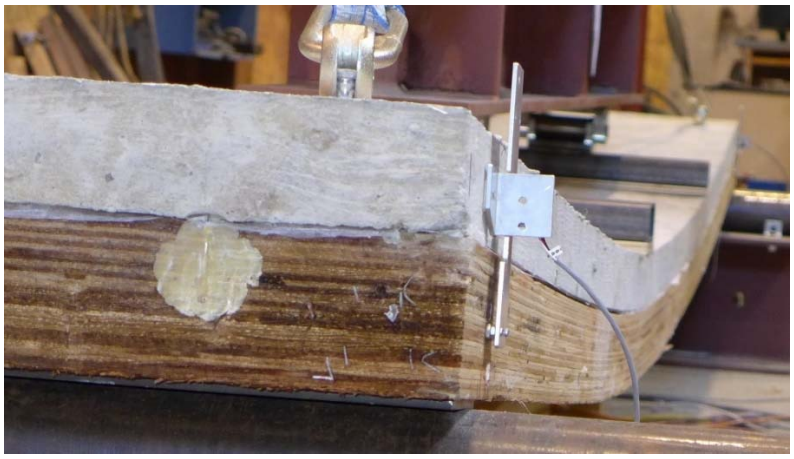

Adam Gerber, EIT, MASc candidate

Version 2, October 30, 2015

Reviewed by:

Thomas Tannert, PhD, PEng

Associate Chair Wood Building Design and Construction

The University of British Columbia

#2933 2424 Main Mall, Vancouver, BC, V6T1Z4, Canada

Phone: (604) 822 1334

thomas.tannert@ubc.ca

http://tannert.forestry.ubc.ca/

Executive Summary

Timber-Concrete-Composite (TCC) systems, specifically the structural performance of different connector types in three engineered wood products (EWPs), were investigated at the University of British Columbia Vancouver (UBC) funded through FII and NSERC.

Small-scale shear tests were performed to evaluate the performance of a wide variety of connectors and to optimize the design of subsequent vibration and bending testing of 6 meter span panels using nine different connection configurations, as summarized in Table 1.

The test program proved that efficient composites can be obtained using any of the available EWPs and connectors. The choice for a specific combination of products can be made based on cost, architectural intent, installation conditions and structural considerations.

Table 1: Results summary

Series	Connector	EWP	Stiffness (10^{12} Nmm^2)	Strength (kNm/m)	Frequency (Hz)	Failure mode
S1	Screws at 30^0	LSL	3.32	192.1	7.1	concrete crushing
S2	Screws at 30^0	LVL	3.82	195.1	7.8	screw withdrawal & timber fracture
S3	Screws at 30^0	CLT	3.03	132.6	6.9	timber fracture
S4	Screws at 45^0 + insulation	LSL	4.50	182.0	8.2	screw withdrawal
S5	Screws at 30^0 + adhesive	LVL	4.04	152.4	7.8	bond failure, screw withdr. & timber fracture
S6	HBV mesh	LSL	3.25	138.3	7.1	connector yielding
S7	HBV mesh	LVL	4.05	139.9	8.0	connector yielding
S8	HBV mesh	CLT	3.04	126.2	7.2	timber fracture
S9	HBV mesh + insulation	LVL	5.93	141.6	9.2	connector yielding

Acknowledgements

This project would not have been possible without the generous contributions of many parties. The industry support allowed us to perform a comprehensive study that is expected to provide a meaningful contribution to the development and use of TCC systems in Canada. The help of the students from Dr. Tannert's research team, Adam Gerber's colleagues and friends, and the technicians at the UBC and FPInnovations laboratories is greatly appreciated.

Funding Partners:

Forest Innovations Investment through Wood First Program

NSERC through Engage program

Industry Sponsors:

Weyerhaeuser – official NSERC partner and sponsorship of LSL

Louisiana Pacific – sponsorship of LVL

Brisco Manufacturing – sponsorship of vertically laminated LVL

Structurlam Products – sponsorship of CLT

MyTiCon – sponsorship of self-tapping screws and FT connectors

TiComTec – sponsorship of HBV mesh

Sika Canada – sponsorship of adhesive

Lafarge – sponsorship of concrete

Collaborators:

FPInnovations – full scale testing

UBC Centre for Advanced Wood Processing –fabrication of test specimens

Equilibrium Consulting – design considerations

Table of Contents

Chapter 1: Introduction

1.1 Background

Timber-Concrete Composite (TCC) systems have been employed as an efficient solution in medium span structural applications; however, their use remains mostly confined to European countries. TCC systems are generally comprised of a timber and concrete element with a shear connection between. A large number of precedents for T-beam configurations exist; however, the growing availability of flat plate engineered wood products (EWPs) in North America has offered designers greater versatility in terms of floor plans and architectural expression in modern timber and hybrid structures. The opportunity exists to enhance the strength, stiffness, fire, and vibration performance of floors using these products by introducing a concrete topping, connected to the timber to form a composite.

The shear connections in TCCs can be achieved using either discrete or continuous connectors that are located according to the expected shear forces. In the case of a simple supported beam with uniformly distributed loads, it is most efficient to locate more connectors near the supports where the shear forces are maximum. The structural efficiency of TCCs depends on the stiffness and strength of the connectors. Systems that exhibit a high degree of composite action benefit from reduced section depths and improved performance by ensuring the complete concrete layer is in compression, thereby preventing cracking. Efficiency can be calculated as the experimentally determined effective bending stiffness, $(EI)_{eff}$, over the computed reference bending stiffness of a composite section connected perfectly rigidly, $(EI)_{ref}$.

1.2 Structural design of TCC

In the case of semi-rigid connectors, which constitute the vast majority that are currently available, a relative slip between the concrete and timber layers will occur. This slip violates the Euler-Bernouli assumption that plane sections remain plane, and therefore requires an alternative to the transformed section method commonly known to structural designers for the determination of bending stiffness and stress distribution of composite sections. Additionally timber, concrete and connectors all exhibit varying time-dependent properties related to creep and shrinkage. The structural design of any TCC design must take into account these two aspects.

A linear-elastic solution, initially proposed by Möhler (1956) for the analysis of timber-timber composite beams, was later recommended by Ceccotti (2002) for use in the analysis of TCC. The assumption that all materials (timber, concrete and connector) remain elastic allows for accurate determination of stresses in composite elements at different load states. The effect of non-linear behaviour of the connector is captured by using its tangent stiffness (determined from tests according to EN 26891 (CEN 1991) in calculations at serviceability and ultimate limit states (SLS and ULS) to predict the stress distributions in the concrete and timber elements and the deflections of the TCC system.

This approach, commonly known as the gamma method, is incorporated into Annex B of Eurocode 5 Part 2 (CEN 2004). The effective flexural rigidity of this system $(EI)_{eff}$ is:

$$(EI)_{eff} = (EI)_0 + \gamma[(EI)_\infty - (EI)_0] \quad (1)$$

where $(EI)_\infty$ is the flexural rigidity for full composite action, $(EI)_0$ is the flexural rigidity if there is no composite action at all, and γ is the gamma factor:

$$\gamma = \frac{1}{1+\frac{\pi^2 (EA)_r}{kl^2}} \quad (2)$$

where l is the beam span, k is the connector stiffness and:

$$(EA)_r = \frac{E_1 A_1 \times E_2 A_2}{E_1 A_1 + E_2 A_2} \quad (3)$$

Importantly, $(EI)_{eff}$ depends on the load distribution and span so it is not a fundamental cross-sectional property (Ceccotti 2002). Furthermore, the solutions generated by this method are exact for simply supported beams with a sinusoidal bending moment along its length; the solutions for other boundary and loading conditions are approximations only.

The gamma method assumes a continuous shear connection; however "smearing" the connector properties across the spacing interval has been shown to provide reasonably accurate results. For cases where connectors are not evenly distributed, Ceccotti (2002) proposed an effective spacing to be used in the calculation of γ:

$$s_{eff} = 0.75 s_e + 0.25 s_m \quad (4)$$

with $s_e < s_m < 4s_e$; s_e and s_m are the spacing at the ends and the middle of the beam respectively.

In addition to the gamma method, finite element modeling can be utilized to provide very accurate predictions of composite sections under any loading scenario. Timber and concrete elements are generally modelled as elastic and the shear connectors are modelled as either linear or non-linear springs depending on the intent of the analysis and the information available.

1.3 Connector types

Ceccotti (2002) divides connectors into four categories that range from relatively weak and flexible connectors such as dowels or nails to very stiff connectors such as glued in plates or notches cut into the timber. Figure 1 illustrates the relative influence of connector stiffness on the γ values (see Equation 3) and the composite efficiency (see Equation 1).

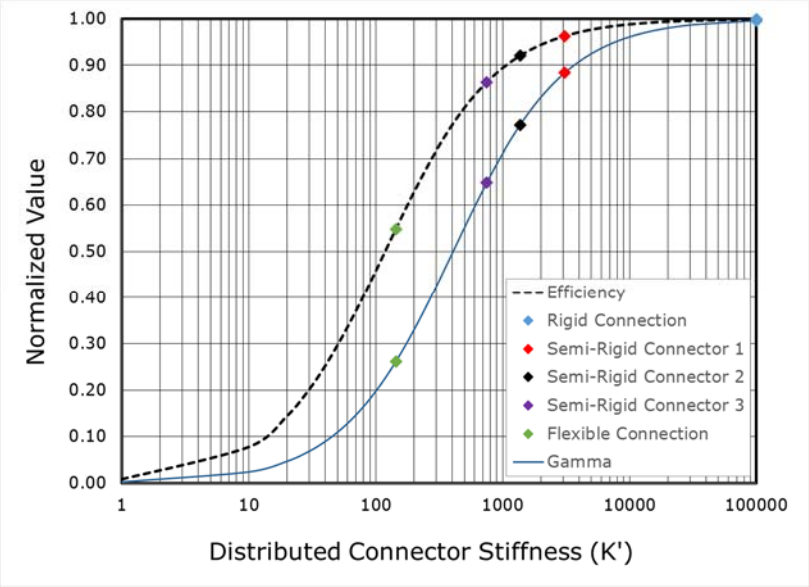

Figure 1: Normalized stiffness vs. composite efficiency and connection stiffness

What can be seen from Figure 1 is that a perfectly rigid connector (i.e. γ=1.0) is not required to achieve a highly efficient composite, and that the biggest gains in efficiency are made by going from a very flexible connector to a relatively stiff connector. This way, TCC systems with greater than 90% efficiency can be obtained economically. It should be noted that high connection stiffness, and consequently composite efficiency, can be achieved by either few very stiff connectors or many less stiff connectors (achieved by reducing connector spacing within rows or adding more rows of connectors).

The performance characteristics of connectors (strength, stiffness and ductility) for serviceability and ultimate limit states (SLS and ULS), can be determined through direct shear push-out tests according to EN 26891 (CEN 1991). Based on the load-slip response of the specimens, tangent stiffness and strength are determined at 40, 60 and 80% of the failure load corresponding to the SLS, ULS and near-collapse loads, respectively (Khorsandnia et al. 2012).

1.4 Research need and project objectives

From conversations with Canadian engineers and designers, it became clear that several issues create barriers to the widespread implementation of TCC in North America.

- Lack of Canadian design approach
- Lack of appropriate test data in North American EWP's
- Lack of readily available connector properties (majority of connector systems are proprietary and cannot be easily compared across the range of materials)
- Uncertainty regarding the long-term performance of TCC systems.

To address these issues, a test program for TCC was developed at UBC to systematically address all of the identified barriers to TCC implementation for North American engineers, designers and suppliers, thereby creating new opportunities for the utilization of timber and providing another potential layer of value-added services to the industry. The test program consisted of three phases:

- Phase I: Small-scale specimens were tested in shear with over 30 configurations of connections and EWP's to collect and analyze strength and stiffness data.
- Phase II: Based on the results of the small-scale tests, nine TCC systems were selected and full-scale specimens were designed, fabricated and tested to validate design assumptions, on stiffness, strength, and vibration properties of the selected TCC systems.
- Phase III: One replicate of each TCC system tested in full scale are being subjected to long-term loading to investigate creep performance.

The results from Phase II are presented in full, while from Phase I only the relevant information to estimate the performance of the full-scale prototypes will be presented. All data on all connector configurations tested in Phase I can be obtained from Adam Gerber's MASc thesis.

Phase III was initiated through a second NSERC Engage grant with Equilibrium Consulting as industry partner. Nine full-scale floors are currently loaded and monitored at UBC.

Chapter 2: Materials

2.1 Engineered Wood Products

The efficient implementation of TCC requires the appropriate combination of wood, concrete and connectors, leaving significant opportunity for designers to optimize based on project specific requirements. Several commonly available EWP's were selected to be tested both in small and full scale along with typical concrete mixes. The material's mechanical properties as summarized in Table 2 are taken from the manufacturer's specifications: (CCMC 12627-R (2015) for LSL, CCMC 11518-R (2015) for LVL, and CrossLam™ Design Guide Version 11 (2015) for CLT.

Table 2: EWP Properties

		Material Properties (MPa) [1]					
Material	Supplier	MOE	F_t	F_c	F_b	F_v	F_{cp}
LSL (1.55E)	Weyerhaeuser	10,685	20.4	22.6	33.3[2]	1.95[2]	6.10[2]
LVL (1.55E)	LP Corp.	13,790	18.6	9.4	37.6[2]	1.79[2]	9.41[2]
CLT (SPF No.1/No.2)	Structurlam	9,500	5.5	11.5	11.8	0.50[3]	--

(1) MOE = Modulus of elasticity; F_t, F_c, F_b, F_v, F_{cp} = specified strengths in tension, compression, bending, shear, and compression perpendicular to grain respectively.

(2) Strength properties for plank orientation

(3) Rolling shear (Longitudinal shear = 1.5 MPa)

2.2 Concrete

Normal strength concrete was used to in order to ensure compatibility with local construction and design practice. The properties listed in Table 3 are those provided by the supplier.

Table 3: Concrete properties

Material	Supplier	f'_c[1] (MPa)	Max aggregate size (mm)	Weight
Ready-Mix Concrete	Lafarge	30	19	Normal

(1) Average cylinder strength at time of testing = 45.5 MPa

2.3 Insulation

Insulation is sometimes desired for enhanced acoustic performance of TCC floors. The layer of insulation also increases the lever arm between the timber and concrete without adding any significant weight. In this way it is possible to increase the stiffness of the panel and potentially improve the vibration performance provided the shear connector can connect effectively through the insulation. In this project, Foamular® C-200 extruded polystyrene rigid insulation was utilized, which is commonly available and has a compressive strength of 140 kPa according to the manufacturers Technical Bulletin No. SC33 (2009).

2.4 Adhesive

Investigation of adhesive bonded TCC panels required the specification of a moisture insensitive adhesive that is capable of bonding wet concrete to timber. Sikadur®32 Hi-Mod was selected, a moisture insensitive, two component structural epoxy suitable for bonding fresh, plastic concrete to hardened concrete and steel or as a structural adhesive for concrete, masonry, metal, and wood. According to the Sikadur®32 Hi-Mod product data sheet (2012), it has a shear strength after 14 days of 41 MPa and a pot life of 30-38 minutes.

2.5 Connectors

A large number of connectors are available for the implementation of TCC, the focus was limited to those which are able to achieve high stiffness and therefore higher composite efficiency. Of almost equal importance as the structural performance of the connectors is the potential for a cost-effective implementation. Five main connector types were investigated which included: i) adhesive bonded steel mesh, ii) fully and partially threaded self-tapping screws, iii) epoxied and hybrid epoxied and screwed connections, iv) FT connector and v) mechanical interlocking.

Within the TCC systems, additional parameters were varied which included: EWP type, presence of slip membrane, presence of rigid insulation interlayer, screw angle, screw embedment length, and screw diameter. Based on the small-scale shear tests as discussed in chapter 3, only the first three connector options were selected to be applied in the full-scale bending tests.

Self-tapping screws

Self-Tapping Screws (STS) do not usually require pre-drilling and are therefore faster to install than traditional lag screws or wood screws, making them a cost efficient connector appropriate for many timber structures. STS with continuous threads are hardened to produce a high yield moment, tensile, and torsional strength. Fully threaded STS (SWG Assy VG) with 10 mm diameter and 240 mm long were used. The technical specifications of the screws are provided by report 13677-R from the Canadian Construction Material Centre (CCMC 2013).

HBV mesh

The proprietary glued-in steel connector system, Holz-Beton-Verbund (HBV) has proven to be among the best options in terms of achieving TCC strength, stiffness and ductility, although there are some concerns regarding the assurance of stringent quality control and complexity of on-site applications. The HBV system has product approvals for being used with epoxy and polyurethane based adhesives (Z-9.1-557, 2012). In the UBC project, CR-421 by Purbond®, a two-component polyurethane adhesive was applied (Lehringer 2012).

Chapter 3: Shear tests

3.1 Specimen configuration

The use of empirical formulae to determine connector stiffness and simplified design procedures, which do not consider non-linear behaviour of connectors, can lead to significant underestimations in connector stiffness and strength and, hence, to larger resistance but brittle failure of the composite beam. The evaluation of the actual connection properties using push-out tests is therefore recommended for the best design of TCCs (Ceccotti et al. 2006).

Test specimens were prepared for more than 30 configurations; herein only those selected subsequently for the full-scale bending tests are presented. They were constructed according to the geometries shown in Figure 2 - Figure 7 and varied according to the parameters described in section 2.5.

HBV mesh

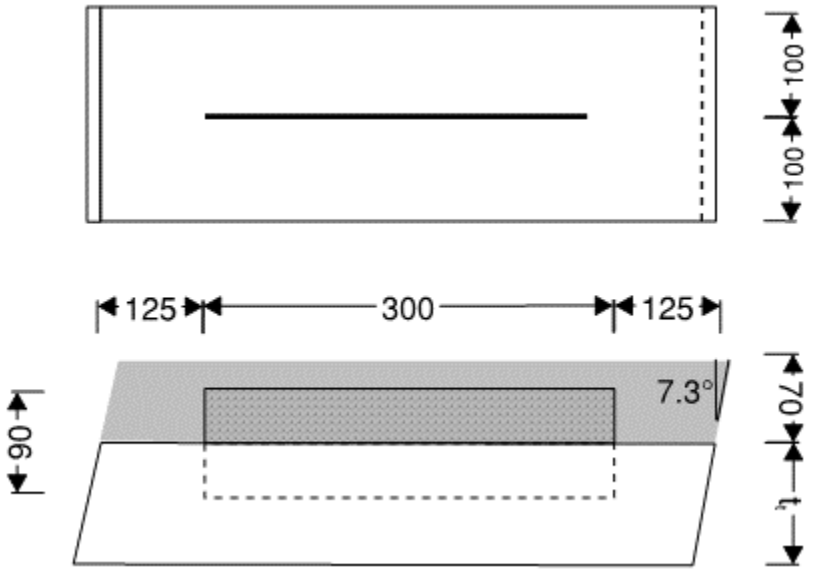

Figure 2: Small-scale shear specimen with HBV mesh

HBV mesh with insulation layer

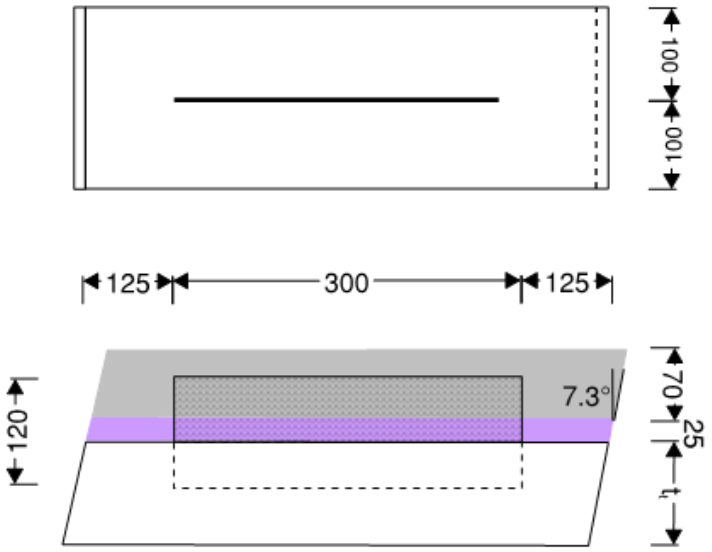

Figure 3: Small-scale shear specimen with HBV mesh and insulation layer

Self-tapping screws at 30°

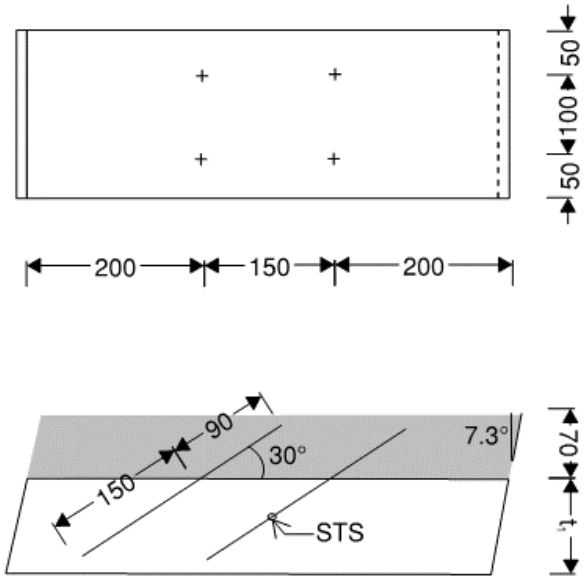

Figure 4: Small-scale shear specimen with STS at 30°

Self-tapping screws in pairs at 45° with insulation layer

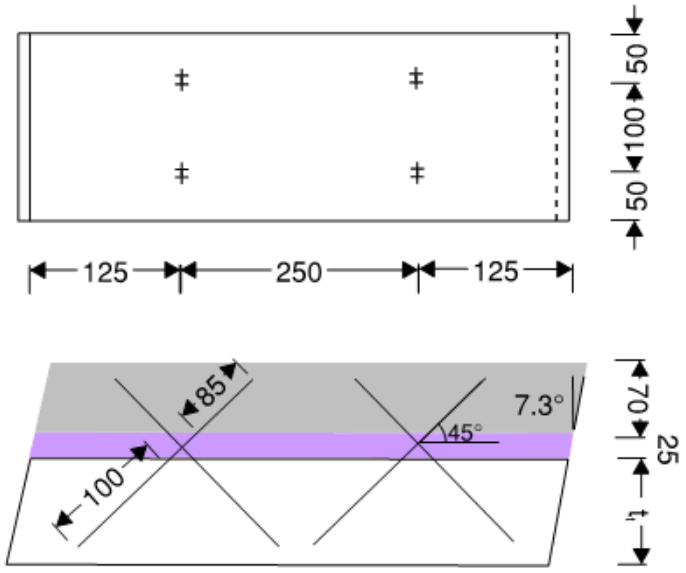

Figure 5: Small-scale shear specimen with pairs of STS at 45° with insulation layer

Connection with adhesive layer

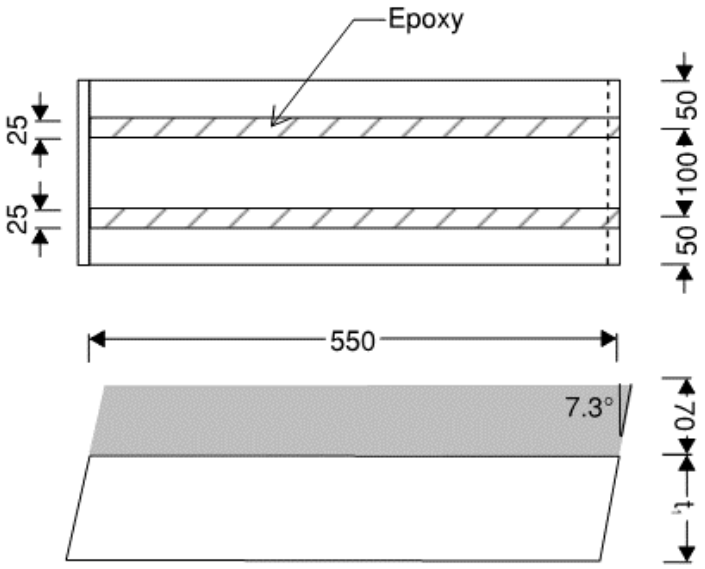

Figure 6: Small-scale shear specimen with adhesive layer

Combination of adhesive layer with self-tapping screws at 30°

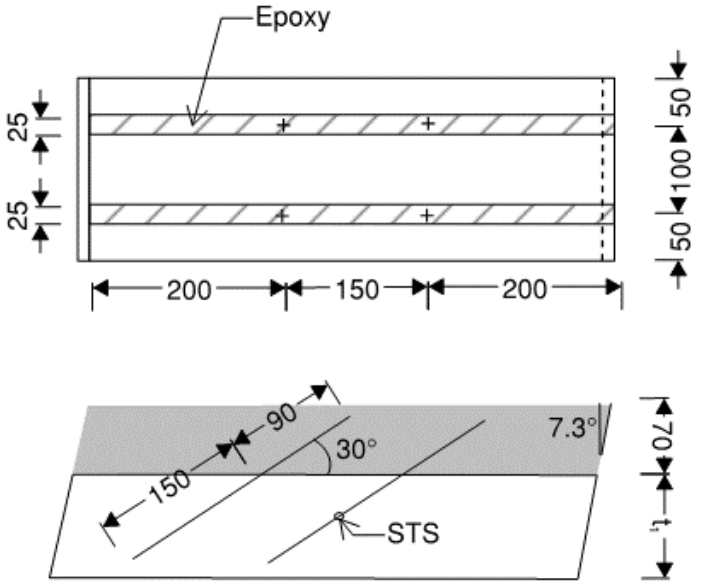

Figure 7: Small-scale shear specimen with epoxy and STS at 30°

3.2 Specimen fabrication

The test specimens were prefabricated at the Center for Advanced Wood Processing (CAWP) at UBC. To the greatest extent possible, specimens were cut on the Hundegger Robot Drive CNC machine according to the geometry shown in Figure 2 - Figure 7. Fabrication was then completed on the table saw and by hand. Typically, a slip membrane was then spray glued to the specimens, after which the connectors were installed using jigs and templates to ensure accurate installation at the angle and spacing specified. Once the connectors were installed, forms were built around them in preparation for concrete casting. Specimens were cast in batches of approximately 30 at a time and then moist cured until testing. Photos of several specimens at various stages of fabrication and/or testing are included in Figure 8.

Figure 8: Shear-test specimens: inclined STS connectors (top) epoxied with STS backup (bottom left), HBV mesh (bottom middle and right)

3.3 Test methods

The shear tests were performed at the UBC Structures Laboratory in a universal testing machine with 400 kip capacity. The load was applied to the specimen through a steel bearing plate on the concrete at the top and the test specimens were supported by another steel bearing plate beneath the timber part of the specimen, see Figure 9. Owing to the skewed geometry, no additional bracing was required for stability.

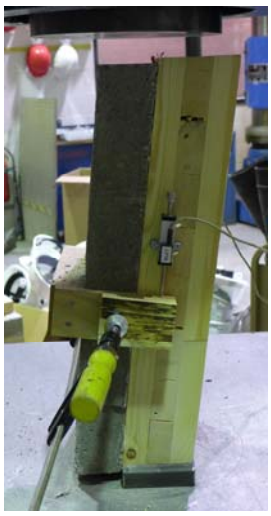

Figure 9: Shear Test Setup

A load-control protocol was implemented according to EN 26891 (CEN 1991) similar to that shown in Figure 10 (left) adapted for the expected loads for each connector type. Specimens were instrumented with linear voltage displacement transducers (LVDTs) on each side to measure the relative slip between the timber and concrete elements with data recorded at a sampling rate of 5 Hz. Figure 10 (right) depicts how the results, as presented in Table 4 & Table 5, were calculated based on the load slip curves.

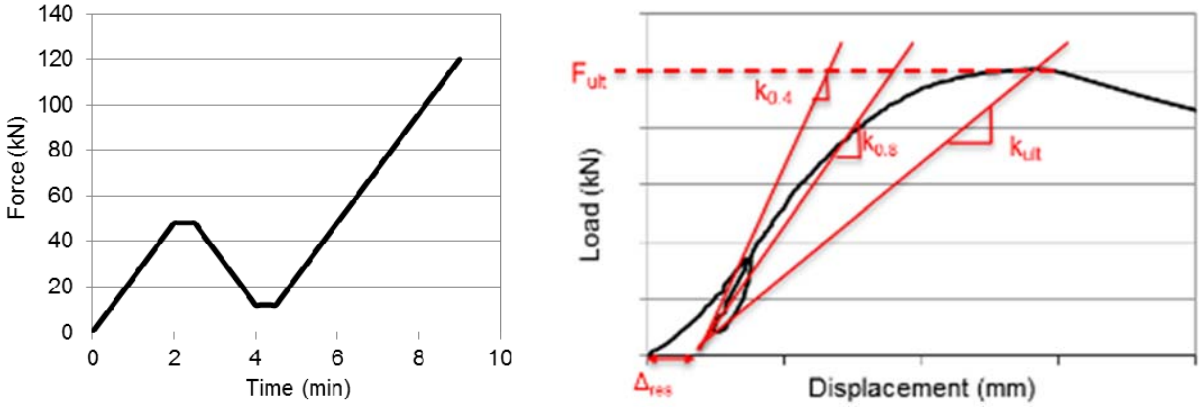

Figure 10: Loading protocol (left) and parameter calculation (right)

3.4 Results

The small-scale shear tests showed that several connector systems are capable of achieving highly efficient composite sections. The HBV mesh, epoxied slabs with backup STS, and cast-in fully threaded STS showed a desirable performance and consequently were selected as the connector types to be implemented in for the full-scale experimental program. These connectors provided high strength and stiffness with little or no residual displacement under service loads; the mean values for strength and stiffness properties are given in Table 4 (per screw) & Table 5 (per 300mm HBV mesh). The complete results from the small scale tests will be presented in Adam Gerber's MASc thesis.

Table 4: Results of small-scale shear tests per screw (or screw pair)

Connector Type	EWP	F_{ult} (kN)	$k_{0.4}$ (kN/mm)	$k_{0.6}$ (kN/mm)	$k_{0.8}$ (kN/mm)	Δ_{res} (mm)
Assy VG CYL 10x240 @ 30°	LSL	32.8	68.7	50.6	39.9	0.11
Assy VG CYL 10x240 @ 30°	LVL	32.2	65.8	42.2	30.8	0.14
Assy VG CYL 10x240 @ 30°	CLT	28.2	72.5	40.9	26.0	0.17
Assy VG CYL 10x240 pairs @ 45° through 25mm insulation	LVL	30.3	62.2	49.7	36.9	0.01
Assy VG CYL 10x240 @ 30° and Sikadur32 Hi-Mod epoxy	LVL	40.9	286.7	237.7	152.4	0.01

Table 5: Results of small-scale shear tests for one 300mm long HBV mesh

Connector Type	EWP	F_{ult} (kN)	$k_{0.4}$ (kN/mm)	$k_{0.6}$ (kN/mm)	$k_{0.8}$ (kN/mm)	Δ_{res} (mm)
HBV mesh (90mm)	LSL	69	462	336	237	0.02
HBV mesh (90mm)	LVL	69	354	282	219	0.01
HBV mesh (90mm)	CLT	72	267	222	165	0.01
HBV mesh (120mm) through 25mm insulation	LVL	57	303	252	204	0.01

Chapter 4: Full-scale bending tests

4.1 Design of specimens

Specimens were designed to exhibit composite efficiencies in the range of 85-95% to allow comparing the connector requirements for similar overall performance. Calculations based on the gamma method were performed along with more detailed FEM models using the software package RFEM 5.04 (2015), which assume elastic concrete and timber elements but account directly for the full non-linear behavior of the connectors. For the purpose of making predictions of experimental results, mean values for strength and stiffness were used. Where only specified values were available, (e.g. EWP's), a coefficient of variation of 10% was assumed to convert 5th percentile values to mean values. A sample γ-method calculation for panel type 1 is presented in Appendix A. Similarly, a summary of the FEM models and parameters is provided in Appendix B. The specific layouts for all five connector types are illustrated in Figure 22 - Figure 33 in Appendix C.

Table 6: Connector Description used for full-scale bending tests

Type	Connector	Description
1	Assy VG CYL 10x240	Installed at 30° angle to the grain (l_{eff} =140mm)
2	Assy VG CYL 10x240	Pairs of screws installed at 45° angle to the grain through 25mm rigid insulation (l_{eff}=90mm)
3	Assy VG CYL 10x240 and Sikadur32 Hi-Mod epoxy	Similar to type 1 plus 2 continuous 50mm wide rows of epoxy adhesive applied wet just prior to casting
4	HBV mesh (90mm)	Installed in 3mm wide saw kerfs bonded with Purbond® CR-421 2-component polyurethane
5	HBV mesh (120mm)	Similar to type 4 plus 25mm rigid insulation interlayer

4.2 Panel specifications

A summary of the panel configurations, including the connector spacing, is presented in Table 7. The parameters t_c, t_t, and t_i refer to concrete, timber and interlayer thickness respectively, while rows refers to the number of rows of fasteners across the width of the panel and s_1 and s_2 refer to fastener spacing in the high and low shear zones of the panel respectively, see Figure 11. The individual drawings for each connector type are shown Figure 22 - Figure 33 in Appendix C.

Table 7: Full-scale panel configurations

Series	EWP	b (mm)	L (mm)	t_c (mm)	t_t (mm)	t_i (mm)	Connector type	s_1 (mm)	s_2 (mm)	rows
S1	LSL	610	6096	70	89	--	1	150	300	3
S2	LVL	610	6096	70	89	--	1	150	300	3
S3	CLT	600	6000	70	99	--	1	150	300	3
S4	LSL	610	6096	70	89	25	2	300	--	3
S5	LVL	610	6096	70	89	--	3	300	--	3
S6	LSL	610	6096	70	89	--	4	--	--	2
S7	LVL	610	6096	70	89	--	4	--	--	2
S8	CLT	600	6000	70	99	--	4	--	--	2
S9	LVL	610	6096	70	89	25	5	--	--	2

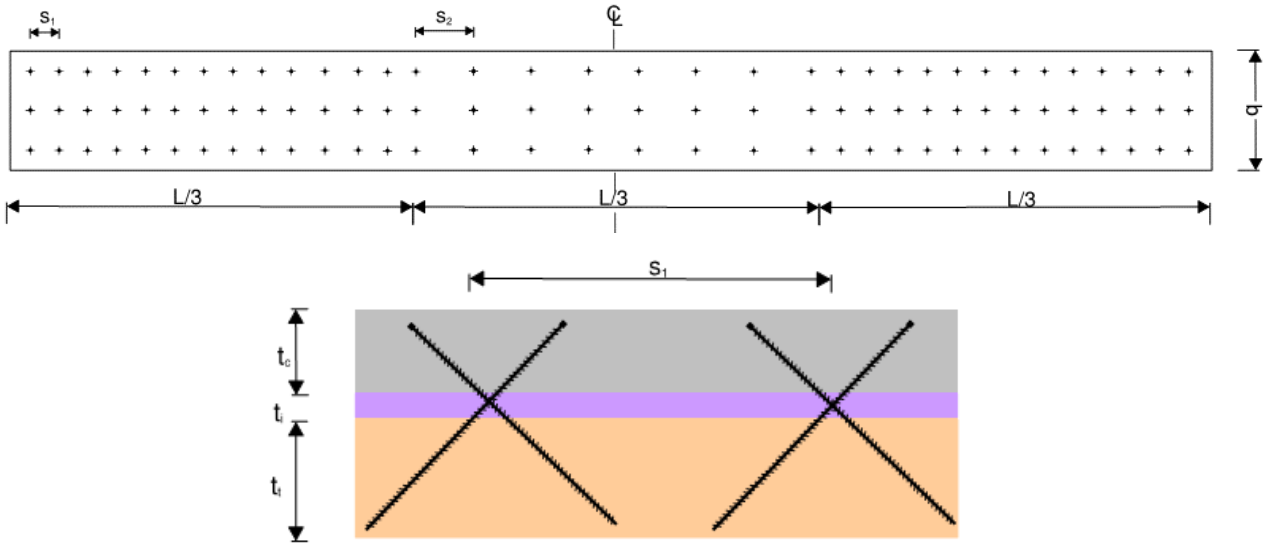

Figure 11: Typical panel dimensions and connector spacings

4.3 Specimen fabrication

All full-scale specimens were prefabricated at CAWP and transported to the FPInnovations yard for casting. The prefabrication process was carried out as follows for the various specimen types:

Self-tapping screw connectors:

- Layout of screw spacing (varied spacing at panel ends and mid-span regions)
- Predrill 6mm pilot holes approximately 40mm deep at prescribed angle (depends on connector configuration and presence of insulation) using hardwood jig
- Install 6 mil poly layer to minimize friction between wood and concrete
- Mark screws using spray paint to ensure proper embedment length
- Install screws using a high torque electric drill until painted portion of screw fully embedded into panel
- Install formwork around panel
- Cut and install WWM reinforcing over screws (centered in concrete depth)

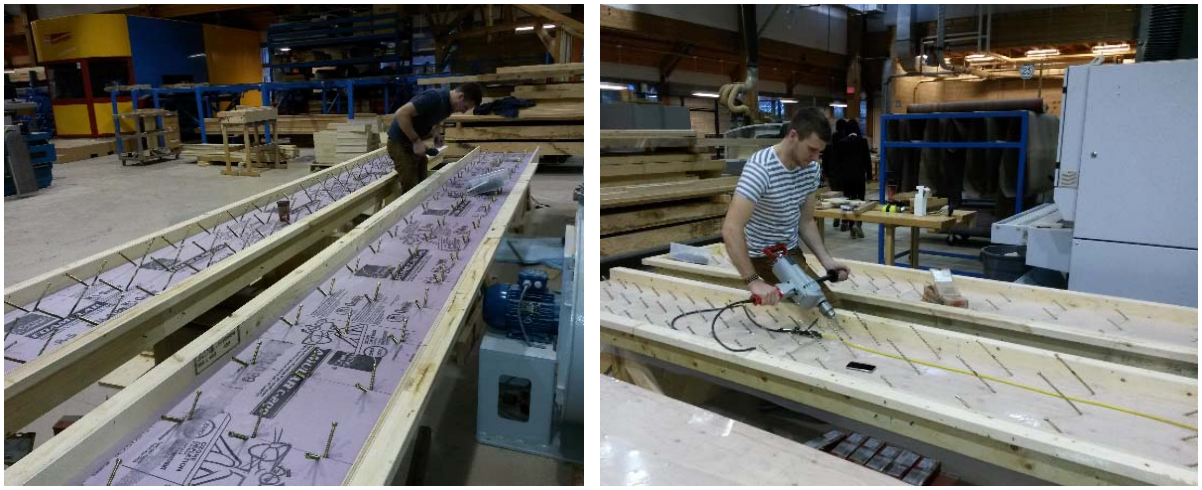

Figure 12: Installation of inclined STS

HBV steel mesh connectors:

- Layout of connector rows
- Cut 45mm deep saw kerfs along length of panel using circular saw with 3mm wide blade.
- Blow out saw kerfs with compressed air and remove saw dust using shop vacuum
- Install 6 mil poly layer to minimize friction between wood and concrete
- Install wood screws at 1 metre intervals to prevent glue seepage and enable sequential connector installation
- Inject two-part polyurethane adhesive supplied by Ti-Com-Tec per manufacturer's instructions into saw kerf intervals followed immediately by installation of steel mesh.
- Install formwork around panel
- Cut and install WWM reinforcing over steel mesh connectors

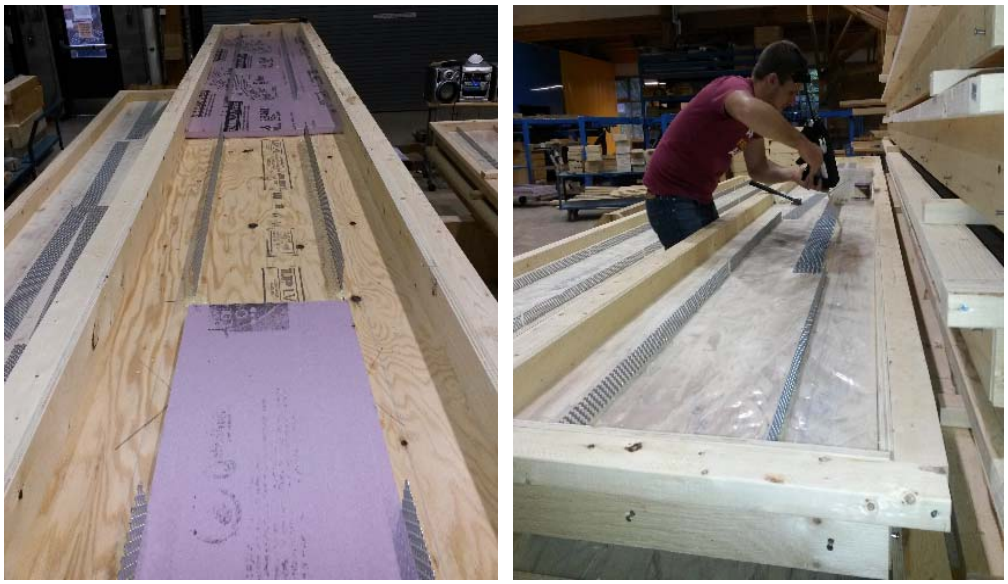

Figure 13: Installation of HBV mesh

Concrete casting:

- All 27 panels were laid out on tarps at the FPInnovations yard for sequential casting with a 10 cubic meter ready-mix delivery truck.
- All formwork had drain holes so that water could not build up in panels prior to casting.
- As panels were poured, they were vibrated, leveled, finished, and covered
- For specimens which were epoxy bonded to the concrete in a wet-wet process, the two part epoxy was mixed just prior to concrete placement and applied to the panel in the appropriate zones.
- 15 test cylinders were also poured at the time of casting and left in the field to cure with the panels for testing near the time of full-scale panel testing.

Figure 14: Concrete casting

4.4 Test set-up

The panels were tested for strength and stiffness under four point bending. The panels spanned 5.8 meters between roller supports to simulate a true simply supported condition. Load was applied to the panel at the third points by a steel spreader beam which was pin connected to a 100 kip hydraulic actuator in a steel reaction frame. The loads were spread evenly across the width of the panel by way of steel HSS tubes. Roller bearings were located between the spreader beam and the HSS tubes ensuring that the specimens were entirely unrestrained by the test apparatus. The complete test apparatus is shown in Figure 15 & Figure 16

Loads were recorded from hydraulic pressures associated with the actuator while vertical displacements were measured by a mid-span LVDT for the stiffness tests and lasers at the mid and third points for the entire test. Four additional LVDTs were installed to measure the relative slip between the concrete and timber at each of the four corners directly over the supports.

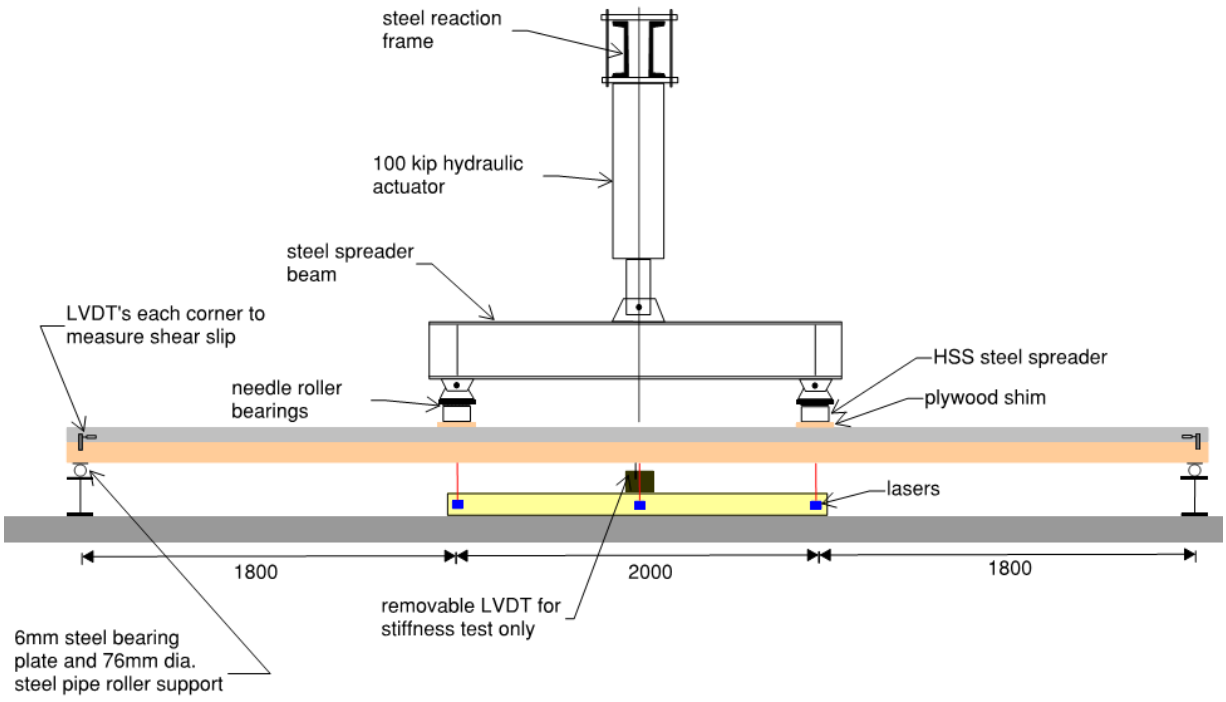

Figure 15: Test setup and instrumentation

Figure 16: Photo of full-scale bending test

4.5 Dynamic test procedure

The dynamic performance of each panel type was predicted based on established methods of mechanics using the effective bending stiffness determined by the γ-method and by dynamic analysis in the FEM software suite RFEM. The panels were initially subjected to dynamic excitation from a light impact (heel strike), and accelerations were monitored using a digital accelerometer. From these acceleration time histories, the fundamental frequency was obtained using a Fast Fourier Transform (FFT). A sample time history and FFT plot are shown in Figure 17. The FFT plot shows each test (i.e. initial, after first service level loading, and after second service loading) and the stabilized natural frequency.

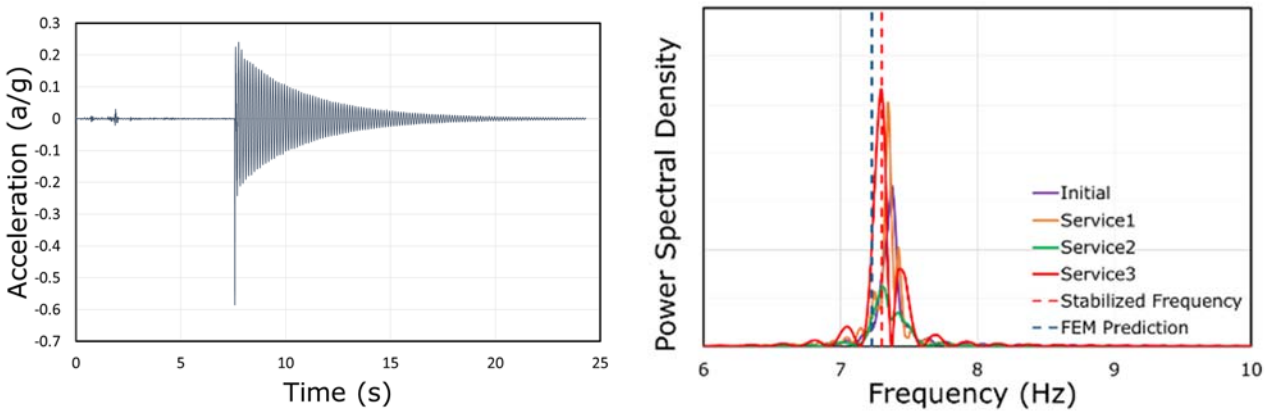

Figure 17: Acceleration time history from heel strike (left) and fundamental frequency determination using FFT (right)

Following the initial vibration test, the panels were loaded to service level (defined as the actuator load causing the same bending moment as would be obtained from a 4.8 kPa UDL), held for thirty seconds, then unloaded a minimum of two times or until the fundamental frequency determined from the vibration tests stabilized. At that point the panel was loaded to failure at a constant displacement rate of 6mm/min. The loading protocol is depicted in Figure 18.

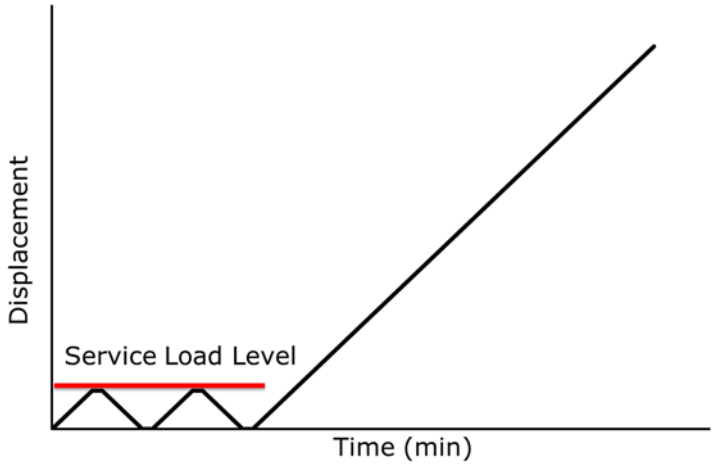

Figure 18: Full scale loading protocol

4.6 Static test procedure

The test procedure for the full scale specimens was adapted from EN 26891 (CEN 1991), the test procedure for small scale shear tests, and extended to include investigations into the dynamic performance of the specimens. TCC connectors show varying degrees of initial inelastic displacement upon first loading, represented by Δr_{es} in the Table 4 Table 5, so an initial loading component was incorporated into the loading protocol to quantify the level of inelastic deflection, (denoted as $\Delta_{inelastic}$ in Table 8), this causes in the panels as well as the potential changes in bending stiffness associated with the inelastic "set" of some connectors. The protocol was further adapted by converting from a load-controlled to displacement-controlled setup.

4.7 Results

Stiffness

The effective bending stiffness, EI_{eff}, inelastic deformation, $\Delta_{inelastic}$, and γ-method and FEM predictions are presented in Table 8. EI_{eff} was calculated based on the initial and service load loading. The inelastic deformation which remained after the initial loading and unloading is reported in the table. The load deformation curves and the load-slip curves for each panel type are given in Appendix D. Results of the dynamic testing for all panels are presented in Table 9.

Capacity and failure types

The results are summarized in Table 10 and each observed failure modes is illustrated in Appendix E. Ultimate load carrying capacity varied between the panel types and was influenced by the failure type. Brittle failure modes such as concrete crushing and tensile fracture of timber elements occurred at much higher loads than more ductile failure modes such as connector yielding or screw withdrawal.

Table 8. Panel stiffness

Series	Replicate	Panel Stiffness - EI_{eff} (x 10^{12} N*mm^2)						
		Measurements		Predictions				
		Initial	Service	FEM	Difference	γ-method	Difference	$\Delta_{inelastic}$
S1	1	3.21	3.41	3.11	-8.7 %	3.24	-5.0 %	1.12
	2	2.78	3.22		-3.3 %		0.7 %	2.10
S2	1	3.61	3.83	3.58	-6.5 %	3.73	-2.6 %	1.11
	2	3.50	3.81		-6.1 %		-2.2 %	1.29
S3	1	2.65	2.90	2.74	-5.5 %	2.84	-2.0 %	1.76
	2	2.83	3.16		-13.3 %		-10.1 %	1.64
S4	1	3.97	4.65	4.39	-5.6 %	4.59	-1.2 %	1.68
	2	4.24	4.34		1.1 %		5.8 %	0.42
S5	1	3.96	4.15	3.78	-8.9 %	3.88	-6.5 %	0.70
	2	3.84	3.92		-3.6 %		-1.1 %	0.21
S6	1	3.36	3.34	3.24	-3.0 %	3.35	0.4 %	--
	2	2.92	3.16		2.6 %		6.1 %	1.42
S7	1	3.79	3.94	3.71	-6.0 %	3.85	-2.4 %	0.73
	2	4.06	4.16		-10.8 %		-7.4 %	0.24
S8	1	3.00	3.13	2.74	-12.5 %	2.85	-8.9 %	0.76
	2	2.89	2.95		-7.3 %		-3.5 %	0.69
S9	1	5.41	5.73	5.60	-2.3 %	5.87	2.4 %	0.58
	2	6.14	6.13		-8.6 %		-4.2 %	0.01

Table 9. Panel vibration results

Series	Replicate	Fundamental Frequency (Hz)				
		Initial	Service_1	Service_2	FEM	γ-method
S1	1	7.37	7.35	7.30	7.14	7.10
	2	7.15	6.98	6.96		
S2	1	7.76	7.66	7.70	7.78	7.75
	2	7.91	7.83	7.81		
S3	1	7.00	6.88	6.84	7.08	7.01
	2	7.12	7.02	6.98		
S4	1	8.35	8.20	8.21	8.48	8.44
	2	8.15	8.13	8.13		
S5	1	7.68	7.70	--	8.05	7.90
	2	7.93	7.93	7.91		
S6	1	7.32	7.32	7.22	7.28	7.21
	2	7.06	7.06	7.03		
S7	1	7.96	7.93	7.93	7.93	7.87
	2	8.10	8.10	8.10		
S8	1	7.28	7.28	7.28	7.08	7.04
	2	7.15	7.13	7.13		
S9	1	9.08	8.88	8.88	9.74	9.71
	2	9.59	9.57	9.55		

Table 10. Panel capacity and failure types

Series	Replicate	P_{max} (kN)	M_{ult} (kNm/m)	Failure type	Description
S1	1	127.2	201.5	brittle	concrete crushing & timber fracture
	2	115.4	182.7	brittle	concrete crushing
S2	1	123.2	191.8	combined	screw withdrawal & timber fracture
	2	127.4	198.4	combined	screw withdrawal & timber fracture
S3	1	74.4	117.8	brittle	timber fracture
	2	93.1	147.3	brittle	timber fracture
S4	1	124.7	197.4	ductile	screw withdrawal
	2	105.2	166.5	ductile	screw withdrawal
S5	1	105.6	164.5	combined	bond, screw withdrawal & timber fracture
	2	90.1	140.3	combined	bond, screw withdrawal & timber fracture
S6	1	89.6	139.5	ductile	connector yielding
	2	88.0	137.0	ductile	connector yielding
S7	1	89.3	139.1	ductile	connector yielding
	2	90.3	140.6	ductile	connector yielding
S8	1	84.5	133.8	brittle	timber fracture
	2	74.9	118.6	brittle	timber fracture
S9	1	91.5	142.5	ductile	connector yielding
	2	90.4	140.7	ductile	connector yielding

Bibliography

Ceccotti, A. (2002). Composite concrete-timber structures. Progress in Structural Engineering and Materials, 4(3), 264-275.

Ceccotti, A., Fragiacomo, M., & Giordano, S. (2006). Long-term and collapse tests on a timber-concrete composite beam with glued-in connection. Materials and Structures, 40(1), 15-25.

EN 1995-1-1 (2004). Eurocode 5: Design of timber structures - part 1.1: General rules and rules for buildings. CEN European Committee for Standardization. Brussels, Belgium:

EN 26891 (1991) Timber Structures, Joints made with Mechanical Fasteners, General Principles for the Determination of Strength and Deformation Characteristics, CEN, Brussels, Belgium.

Frangi, A., and Fontana, M. (2003). Elasto-plastic model for timber-concrete composite beams with ductile connection. Structural Engineering International, 13(1), 47-57.

Gutkowski, R., Brown, K., Shigidi, A., & Natterer, J. (2008). Laboratory tests of composite wood–concrete beams. Construction and Building Materials, 22(6), 1059-1066.

Khorsandnia, N., Valipour, H. R., & Crews, K. (2012). Experimental and analytical investigation of short-term behaviour of LVL-concrete composite connections and beams. Construction and Building Materials, 37, 229.

Lehringer C (2012) PURBOND 2C-Adhesives. Cost action FP 1004 Report. Wrozlaw, Poland

Möhler, K. (1956). "On the load carrying behavior of beams and columns of compound sections with flexible connections." Habilitation, Technical Univ. of Karlsruhe, Germany

Evaluation Report – LP SolidStart LVL (2015). CCMC 11518-R, Canadian Construction Materials Centre, Ottawa, Canada.

Evaluation Report - TimberStrand LSL (2015). CCMC 12627-R, Canadian Construction Materials Centre, Ottawa, Canada.

CrossLam™ Design Guide Metric – Ver 11 (2015). Structurlam Products, Penticton, Canada.

General Certificate of Approval for Holz-Beton-Verbundsystem (HBV), (2012). Z-9.1-557, German Institute for Construction Technology, Berlin, Germany.

Evaluation Report – SWG Assy® VG Plus and SWG Assy® 3.0 Self-Tapping Wood Screws, (2013). CCMC 13677-R, Canadian Construction Materials Centre, Ottawa, Canada.

Ciarlo, S. Allowable Loads on Owens Corning Foam Products (2009), Technical Bulletin No.SC33, Owens Corning

Sikadur 32 Hi-Mod Product Data Sheet Version 1, (2012), Sika Canada Inc., Canada

RFEM structural analysis software, Version 5.04, (2015), Dlubal

Appendix A: Design of full scale specimens according to gamma method

Wood Concrete Composite Beam Design (according to EN 1995 - Appendix B)

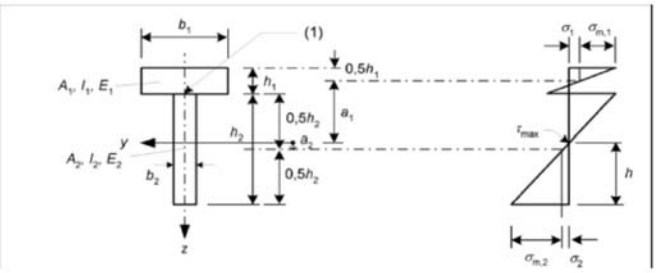

Geometry:

$L := 5.8m$ span

$b := 0.61m$ width

Concrete: (normal weight and strength)

$f_c := 45.45MPa$ $\psi_2 := 0.3$ from Eurocode

$\phi_c := 1$

$f_r := 0.6 \cdot \sqrt{f_c \cdot MPa} = 4.045 \cdot MPa$ modulus of rupture for determination of cracking moment from CSA - A23.3

$E_c := 4500 \cdot \sqrt{f_c \cdot MPa} = 3.034 \times 10^4 \cdot MPa$ elastic modulus of concrete from CSA - A23.3

$k_{def\_c} := 2.5$ deformation factor for long term loading of concrete

$$E_{c\_SLS\_LT} := \frac{E_c}{1 + k_{def\_c}}$$ Effective concrete modulus at long term for SLS

$$E_{c\_ULS\_LT} := \frac{E_c}{1 + \psi_2 \cdot k_{def\_c}}$$ Effective concrete modulus at long term for ULS

$\gamma_c := 23.5 \frac{kN}{m^3}$ specific weight of concrete

$t_c := 70mm$ thickness of concrete

Timber: (1.55E LSL timberstrand by Weyerhaeuser - specified properties from CCMC 08675-R)

$f_b := 33.30MPa$ characteristic bending strength (plank orientation)

$\phi_b := 1$ $\phi_t := 1$ $\phi_v := 1$

$f_t := 20.40MPa$ specified tension strength

$f_v := 1.95MPa$ specified shear strength (plank orientation)

$E_t := 10685MPa$ grade 1.55E

$k_{def\_t} := 0.6$ deformation factor for long term loading of timber

$$E_{t\_SLS\_LT} := \frac{E_t}{1 + k_{def\_t}}$$ Effective timber modulus at long term for SLS

$E_{t\_ULS\_LT} := \frac{E_t}{1 + \psi_2 \cdot k_{def\_t}}$ Effective timber modulus at long term for ULS

$t_t := 89mm$

$\rho_t := 700 \frac{kg}{m^3}$ kg/m3

$\gamma_t := \rho_t \cdot g = 6.865 \cdot \frac{kN}{m^3}$ specific weight of timber

$mc\_t := 12\%$ moisture content of timber

Interlayer Properties:

$t_i := 0mm$ interlayer thickness

Loads:

$DL\_part := 1.0kPa$ specified partition load

$DL_{TCC} := t_t \cdot \gamma_t + t_c \cdot \gamma_c = 2.256 \cdot kPa$ dead load from self-weight

$LL_{2.4} := 2.4kPa$ specified live load

$LL_{3.6} := 3.6kPa$ specified live load

$LL_{4.8} := 4.8kPa$ specified live load

$w_{DL} := (DL_{TCC} + DL\_part) \cdot b = 1.986 \cdot \frac{kN}{m}$

$w_{LL} := LL_{4.8} \cdot b = 2.928 \cdot \frac{kN}{m}$

$w_f := 1.25 \cdot w_{DL} + 1.5 \cdot w_{LL} = 6.875 \cdot \frac{kN}{m}$

Connectors: (Timtec plus VG screws - properties per ETA-12/0196)

$dia := 10mm$ screw diameter (either 8 or 10mm)

$\alpha := 30deg$ inclination angle of screws

$n_r := 3$ rows of screws across width

$s_r := 150mm$ spacing between rows

$l_{sc} := 240mm$ screw length

$k_{def\_con} := 0.6$ deformation factor for long term loading of Timtec plus VG screw connection

$K_{ser} := 68.7 \frac{kN}{mm}$ from test results screw stiffness at SLS for short term loading

$K_{ser\_0.8} := 50.6 \frac{kN}{mm}$ from test results screw stiffness at ULS for short term loading

$F_{Rk} := 32.8kN$ from test results mean value strength from tests

$\phi_{con} := 1$ arbitrary value material strength reduction factor

$$K_{ser\_SLS\_LT} := \frac{K_{ser}}{1 + k_{def\_con}} = 42.938 \cdot \frac{kN}{mm}$$ screw stiffness at SLS for long term loading

$$K_{ser\_ULS\_LT} := \frac{K_{ser\_0.8}}{1 + \psi_2 \cdot k_{def\_con}} = 42.881 \cdot \frac{kN}{mm}$$ screw stiffness at ULS for long term loading

Analysis Results:

$Results\_SLS := parametric\_study\_SLS(F_{Rk}, K_{ser}, \alpha, t_c, t_t, b, f_c, f_r, f_b, f_t, f_v, L, l_{sc}, dia, s, n_r, E_c, E_t, w_f, w_{DL})$

$Results\_ULS := parametric\_study\_ULS(F_{Rk}, K_{ser\_0.8}, \alpha, t_c, t_t, b, f_c, f_r, f_b, f_t, f_v, L, l_{sc}, dia, s, n_r, E_c, E_t, w_f, w_{DL})$

Strength Results:

$conc\_comp := Results\_ULS_1 = 0.346$

$conc\_tens := Results\_ULS_2 = 0.884$

$timb\_tens := Results\_ULS_3 = 0.364$

$timb\_shear := Results\_ULS_4 = 0.151$

$screw\_shear := Results\_ULS_5 = 0.273$

$NA\_SLS := Results\_SLS_6 \cdot t_t = 95.083 \cdot mm$

$NA\_ULS := Results\_ULS_6 \cdot t_t = 93.696 \cdot mm$

$M_{max} := Results\_ULS_9 \cdot kN \cdot m = 32.698 \cdot kN \cdot m$

Stiffness Results:

$Efficiency\_SLS := Results\_SLS_0 \cdot 100\% = 94.209 \cdot \%$

$EI_{eff\_SLS} := Results\_SLS_7 \cdot N \cdot mm^2 = 3.245 \times 10^{12} \cdot N \cdot mm^2$

$\Delta DL\_SLS := Results\_SLS_{11} = 643.031$

$\Delta\_LL_{2.4} := Results\_SLS_{12} = 872.367$

$\Delta\_LL_{3.6} := Results\_SLS_{13} = 581.578$

$\Delta\_LL_{4.8} := Results\_SLS_{14} = 436.183$

$\Delta tot_{2.4} := Results\_SLS_{15} = 370.173$

$\Delta tot_{3.6} := Results\_SLS_{16} = 305.381$

$\Delta tot_{4.8} := Results\_SLS_{17} = 259.892$

Dynamic Properties:

$$m_{tcc} := \frac{DL_{TCC} \cdot b}{g} = 140.326 \frac{kg}{m}$$ mass per unit length

$$M := m_{tcc} \cdot \frac{L}{2} = 406.947\,kg$$ generalized modal mass

$$K := \frac{\pi^4 EI_{eff\_SLS}}{2 \cdot L^3} = 809.932 \cdot \frac{N}{mm}$$ generalized stiffness

predicted SLS natural frequency

$$f_n := \frac{1}{2\pi} \cdot \sqrt{\frac{K}{M}} = 7.1 \cdot Hz$$

$$\sigma_{ULS} := \begin{pmatrix} 0MPa \\ -Results\_ULS_{18} \\ -Results\_ULS_{19} \\ Results\_ULS_{20} \\ -Results\_ULS_{21} \\ 0MPa \end{pmatrix} \quad \sigma_{SLS} := \begin{pmatrix} 0MPa \\ -Results\_SLS_{18} \\ -Results\_SLS_{19} \\ Results\_SLS_{20} \\ -Results\_SLS_{21} \\ 0MPa \end{pmatrix} \quad h_{dist} := \begin{pmatrix} t_t + t_i + t_c \\ t_t + t_i + t_c \\ t_i + t_t \\ t_t \\ 0mm \\ 0mm \end{pmatrix}$$

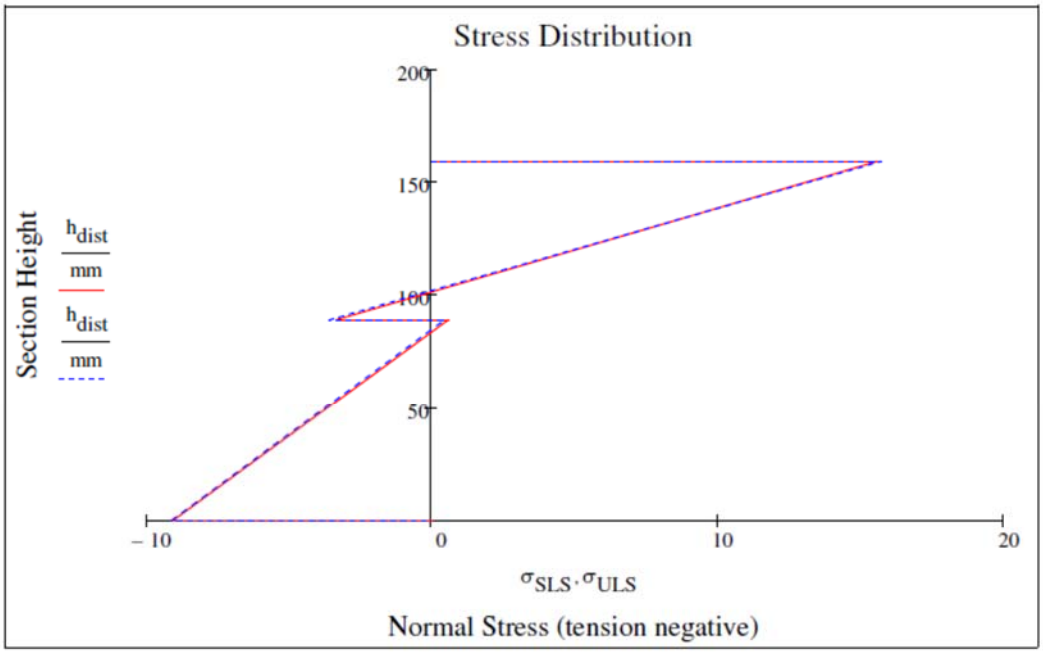

Appendix B: FEM modeling of full-scale panels

The FEM modeling was performed in the software suite RFEM. Each specimen was modeled according to the dimensions and material parameters presented in Table 11. Timber and concrete were modeled as elastic beam elements with their centroids offset by the distance e' as shown in Figure 19. In the case of CLT, a stiffness element was used due to the fact that not the entire section is capable of withstanding tensile stresses and that CLT too has an effective bending modulus due to the cross layers and variations in shear stiffness. The I_{eff_t} and A_{eff_t} parameters refer to the effective moment of inertia and effective tensile area used to model the CLT elements. In order to accurately model the connectors, link elements were connected to springs which lie in the shear plane between timber and concrete. The springs were calibrated according to the stiffness values presented in Table 4 and Table 5 as shown in Figure 21.

Table 11: FEM modeling parameters

Panel Type	t_c (mm)	t_t (mm)	t_i (mm)	e' (mm)	γ_c (kN/m^3)	γ_t (kN/m^3)	E_c (MPa)	E_t (MPa)	I_{eff_t} (10^6 mm^4)	A_{eff_t} (10^3 mm^4)
1	70	89	--	79.5	23.5	6.87	30,337	10,685	--	--
2	70	89	--	79.5	23.5	6.00	30,337	13,790	--	--
3	70	99	--	84.5	23.5	4.12	30,337	9,500	42.2	38.4
4	70	89	25	104.5	23.5	6.87	30,337	10,685	--	--
5	70	89	--	79.5	23.5	6.00	30,337	13,790	--	--
6	70	89	--	79.5	23.5	6.87	30,337	10,685	--	--
7	70	89	--	79.5	23.5	6.00	30,337	13,790	--	--
8	70	99	--	84.5	23.5	4.12	30,337	9,500	42.2	38.4
9	70	89	25	104.5	23.5	6.00	30,337	13,790	--	--

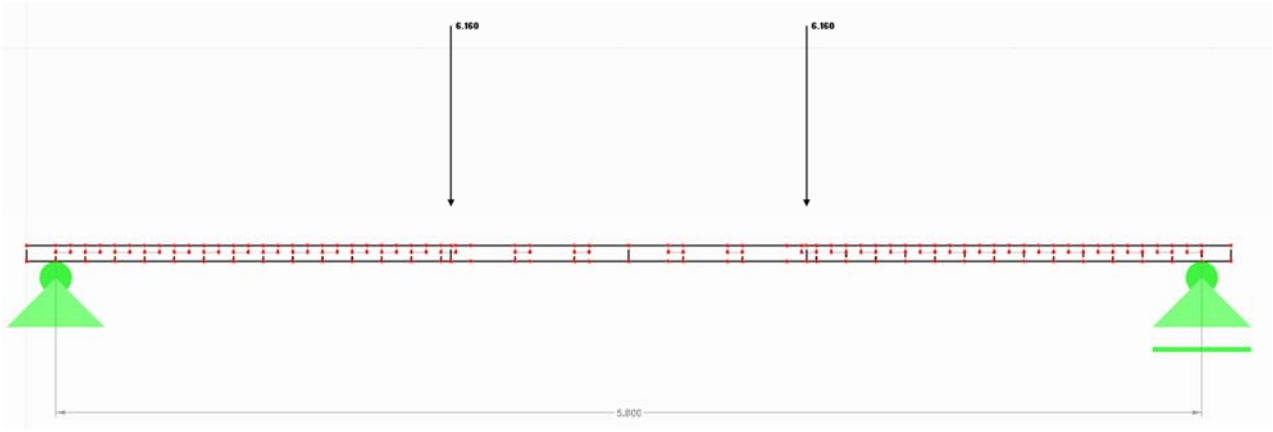

Figure 19: FEM model of test set-up with elastic beam elements and springs at fastener locations

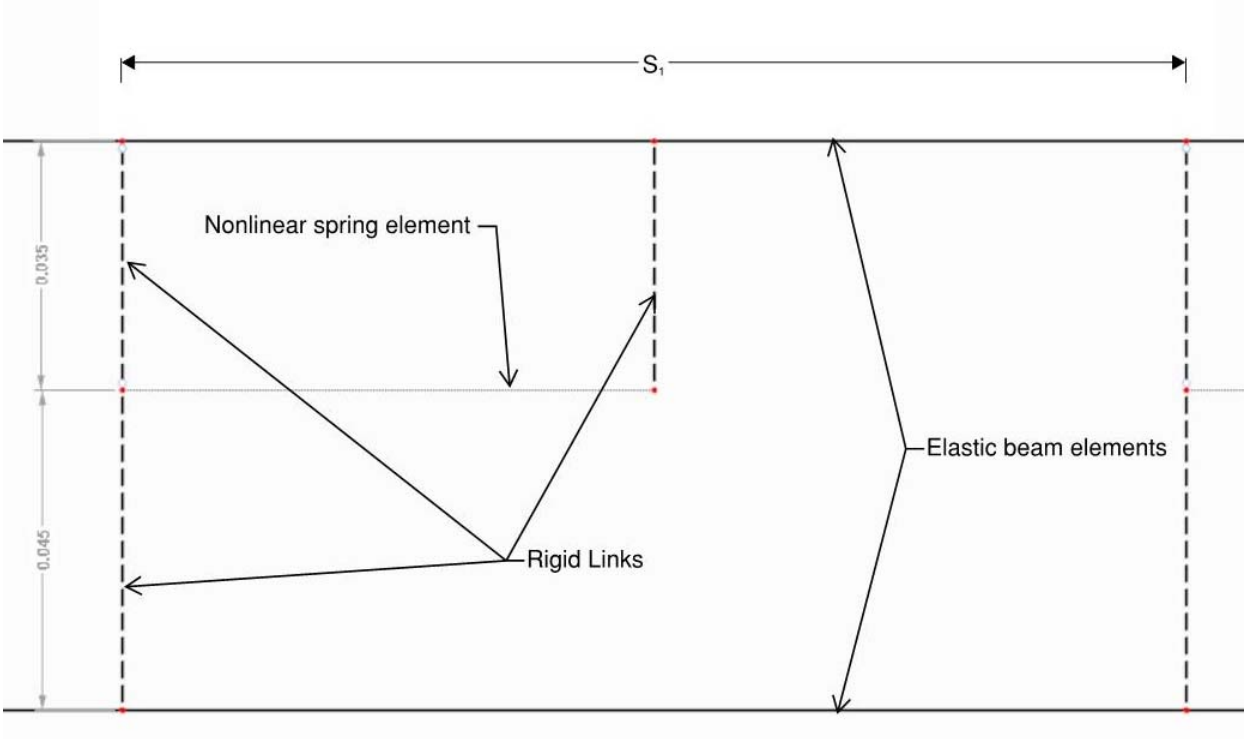

Figure 20: Close up of FEM model at springs

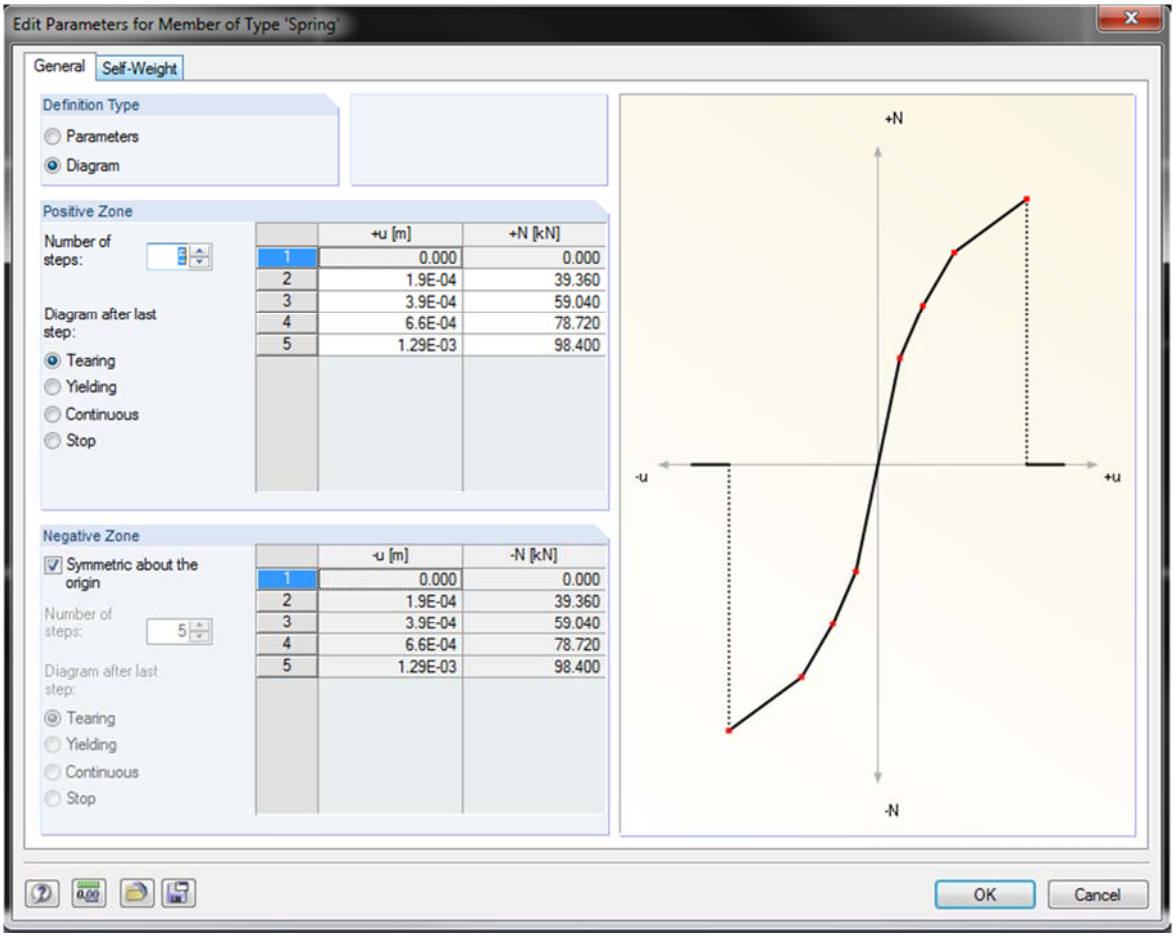

Figure 21: Nonlinear spring calibration

Appendix C: Connector layout drawings

Type 1: Assy VG CYL 10x240 at 30^0

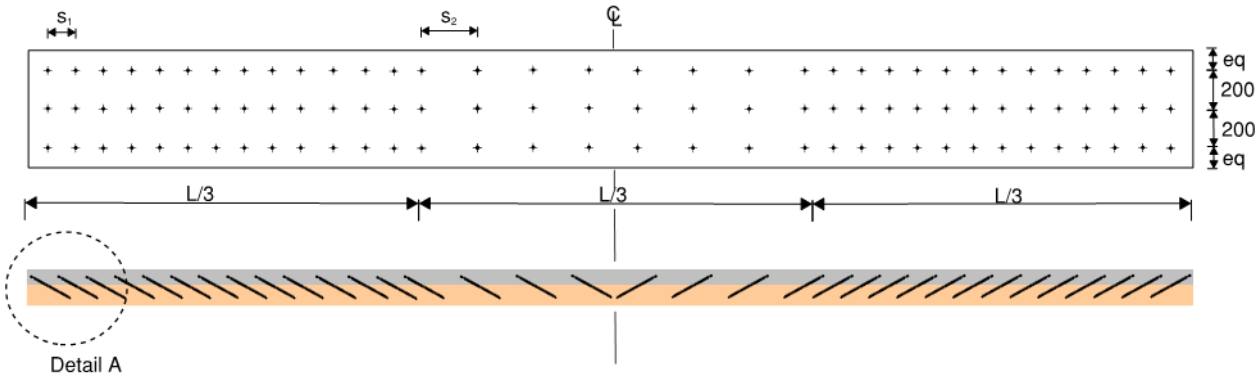

Figure 22: Layout of typical panel with inclined STS (Type 1)

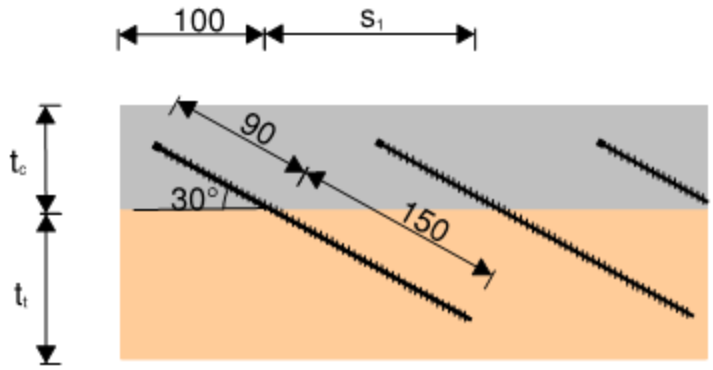

Figure 23: Detail A (inclined STS)

Type 2: Assy VG CYL 10x240 pairs at 45^0 through 25mm rigid insulation

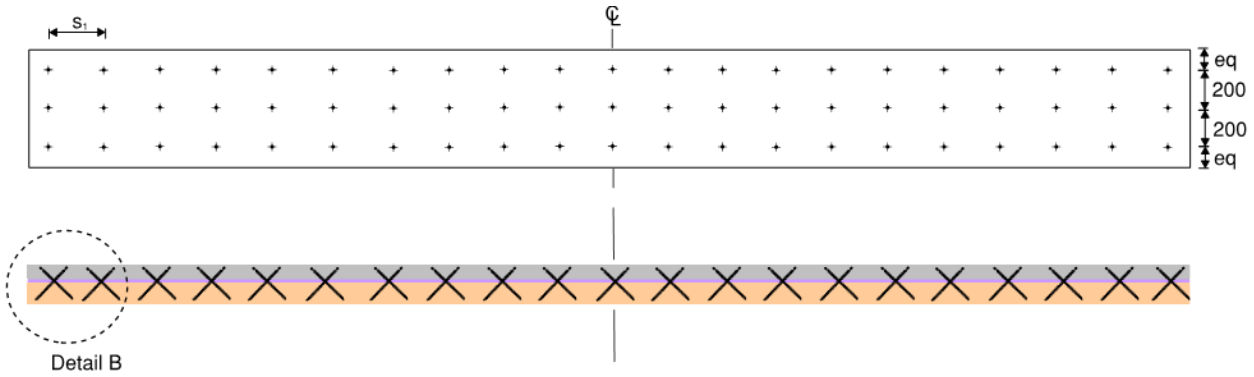

Figure 24: Layout of typical panel with pairs of inclined STS through rigid insulation (Type 2)

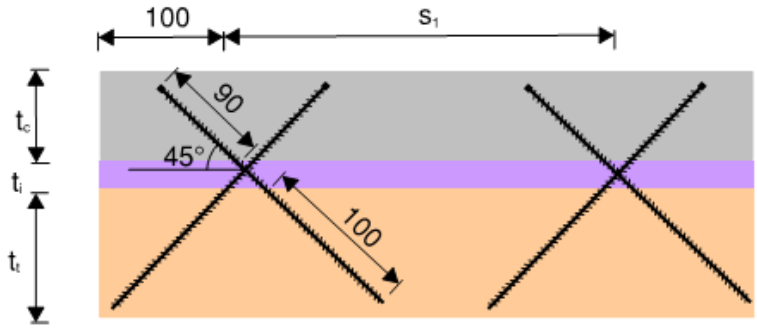

Figure 25: Detail B (pairs of inclined STS through rigid insulation)

Type 3: Assy VG CYL 10x240 at 30^0 plus adhesive layer

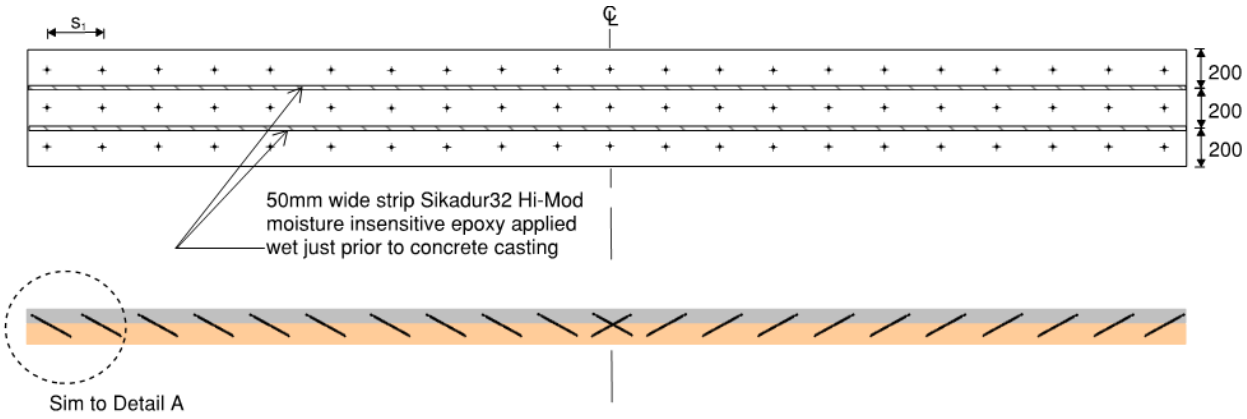

Figure 26: Layout of typical panel with adhesive layer and inclined STS (Type 3)

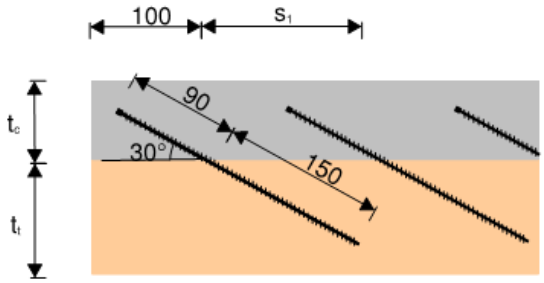

Figure 27: Detail A (adhesive layer and inclined STS)

Type 4: 90mm HBV mesh

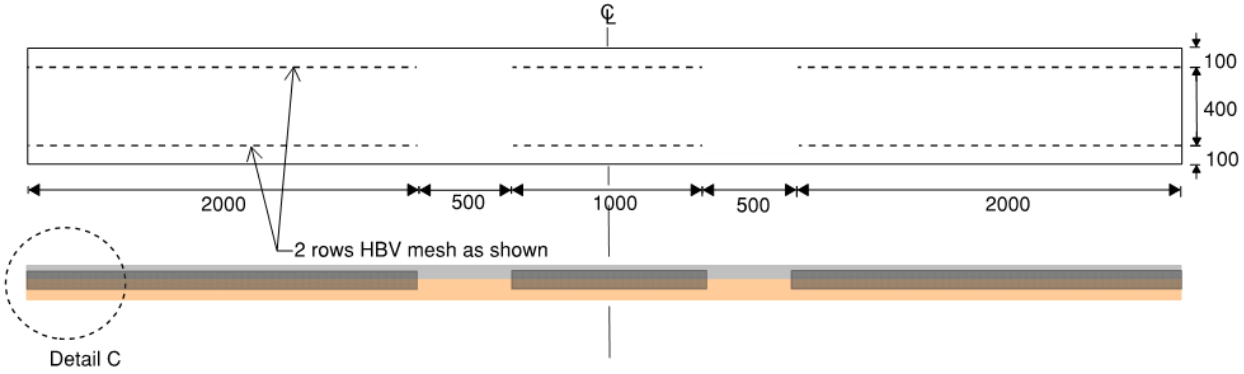

Figure 28: Layout of typical panel with HBV mesh (Type 4)

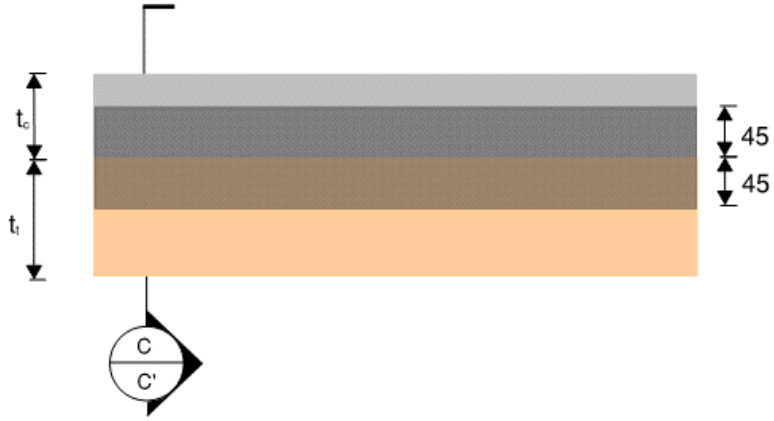

Figure 29: Detail C (HBV mesh)

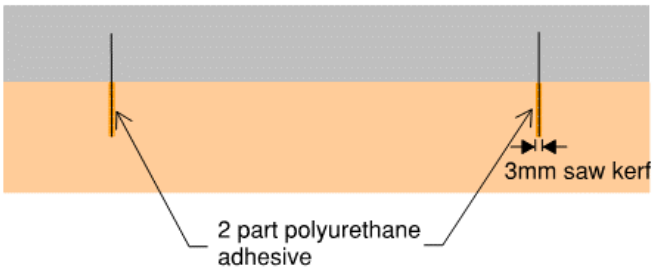

Figure 30: Section C-C` (HBV mesh)

Type 5: 120mm HBV mesh through 25mm rigid insulation

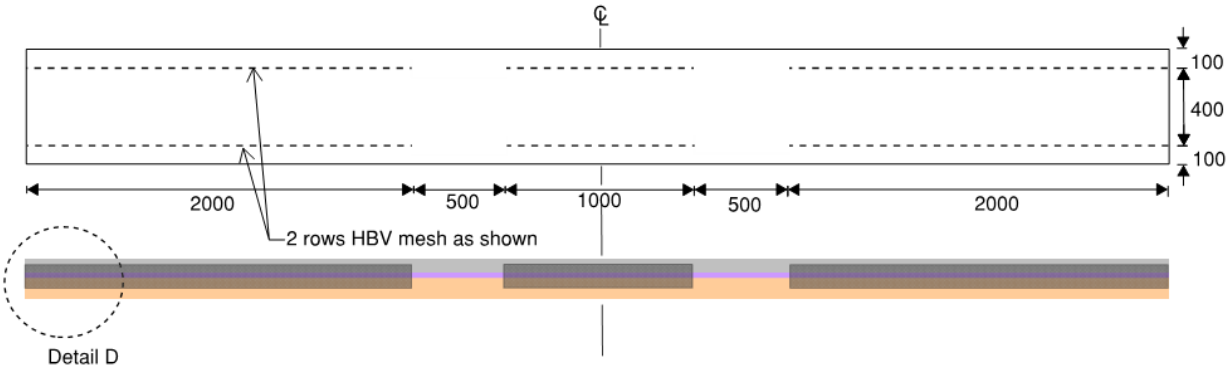

Figure 31: Layout of typical panel with HBV mesh through rigid insulation (Type 5)

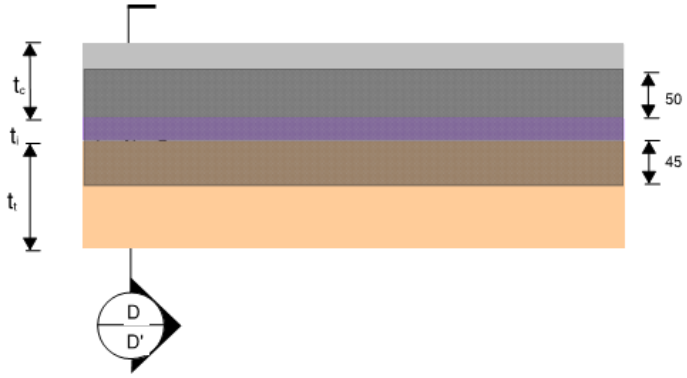

Figure 32: Detail D (HBV mesh through rigid insulation)

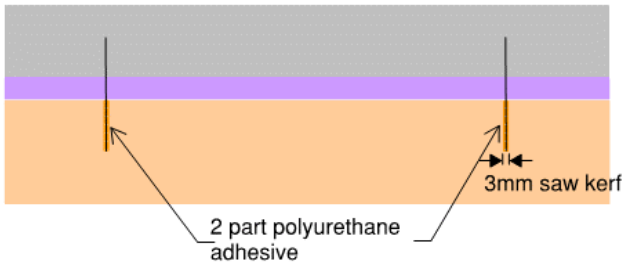

Figure 33: Section D-D` (HBV mesh through rigid insulation)

Appendix D: Load-Displacement Curves

Series 1: Screws installed at 30^0 in LSL

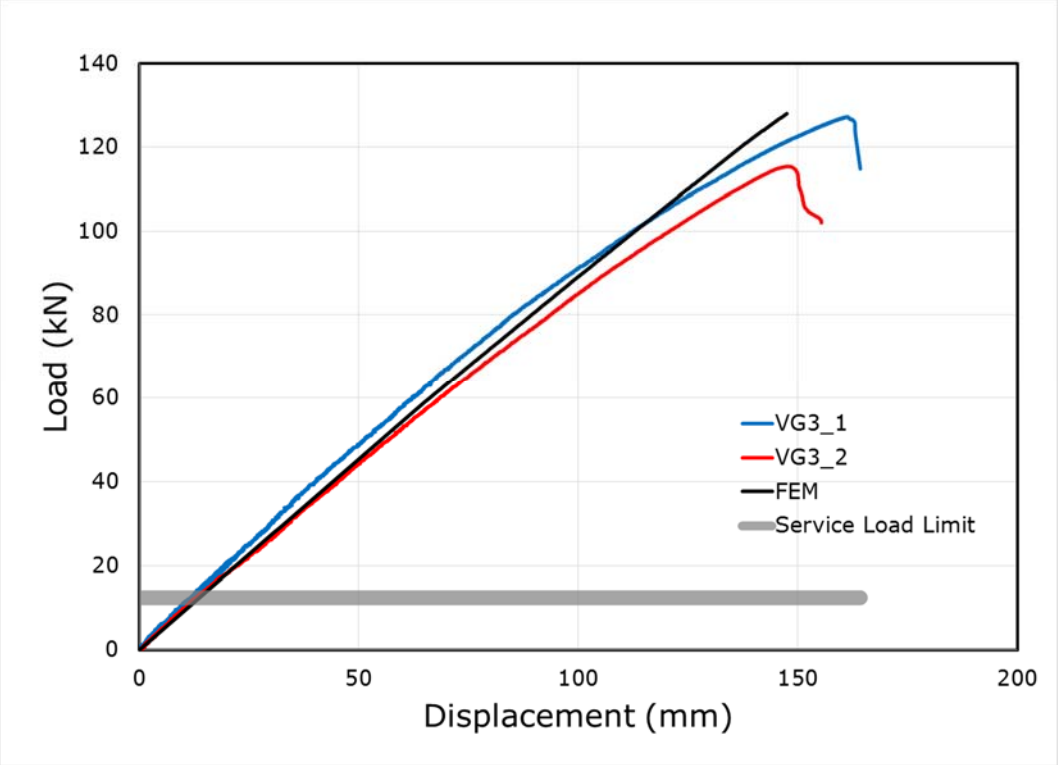

Figure 34: Load vs. Displacement of Series 1

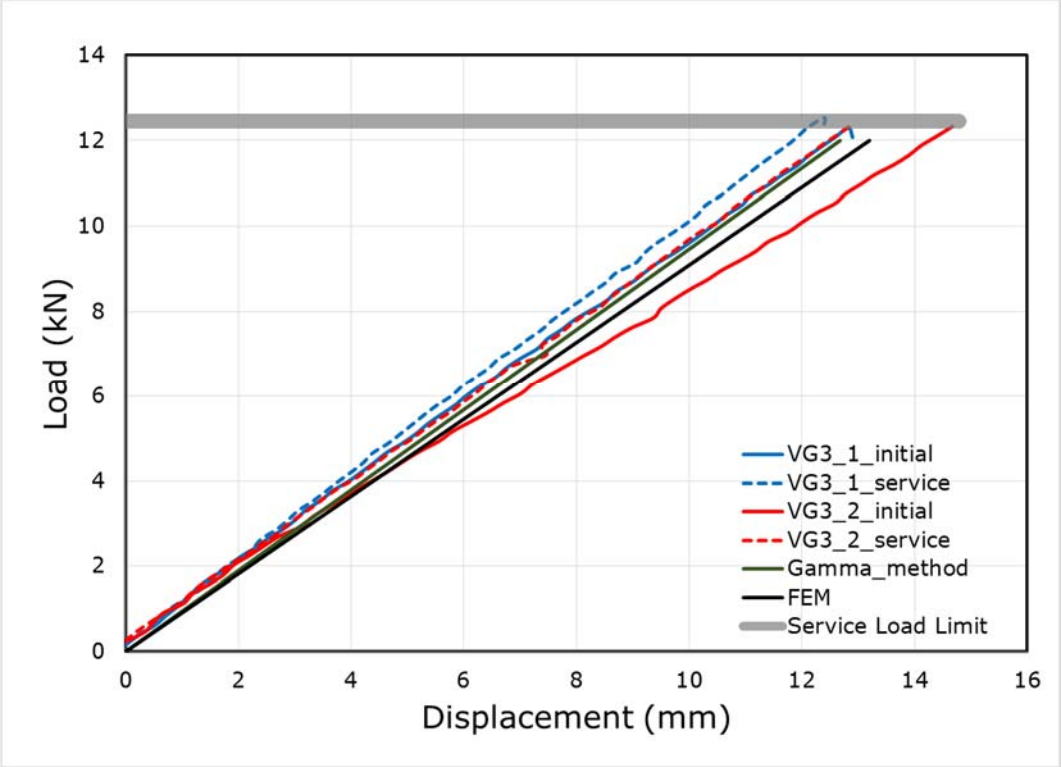

Figure 35: Load vs. Displacement of Series 1 up to Service Level

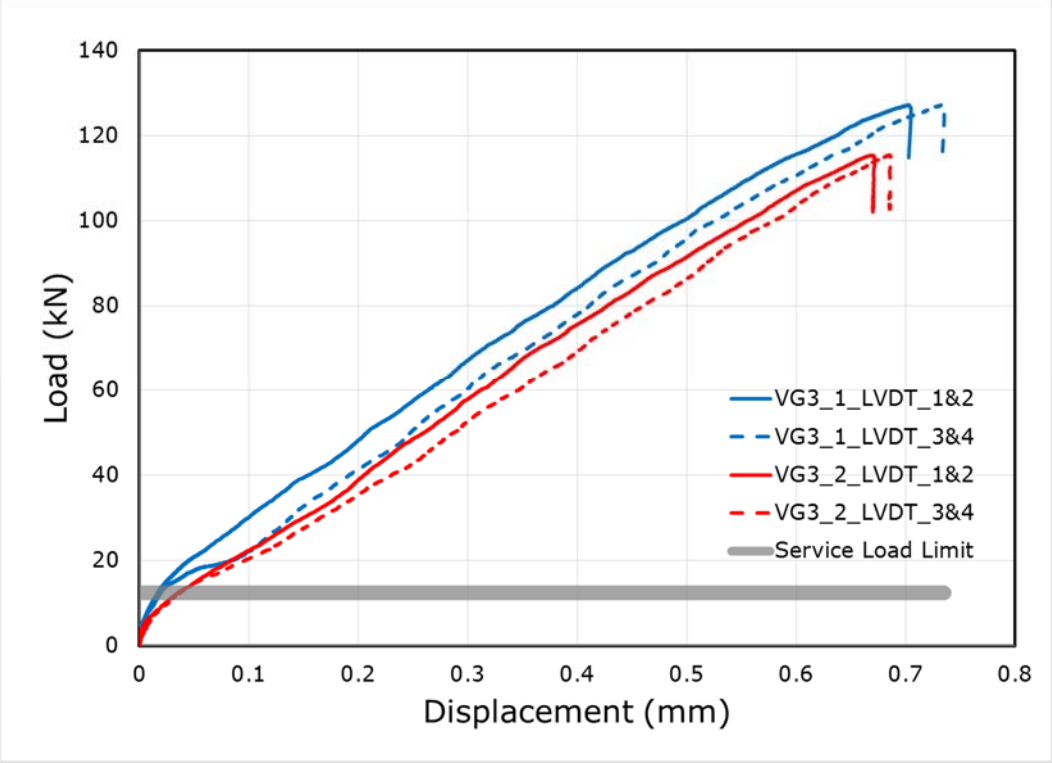

Figure 36: Load vs Shear Slip of Series 1

Series 2: Screws installed at 30^0 in LVL

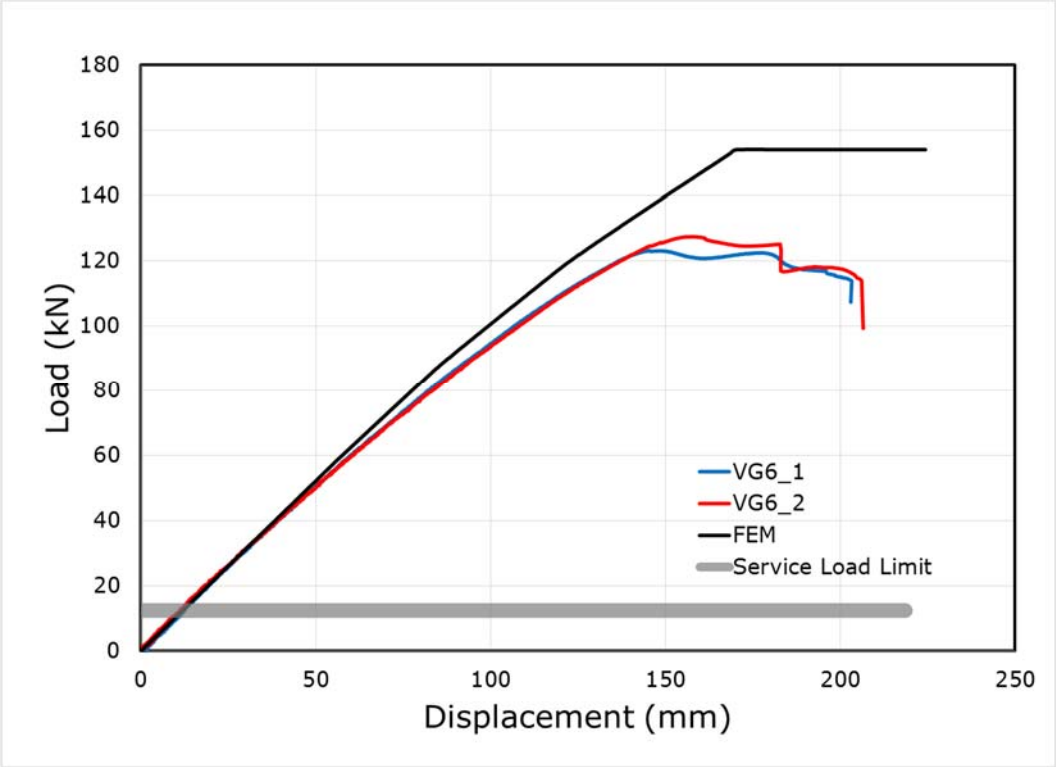

Figure 37: Load vs. Displacement of Series 2

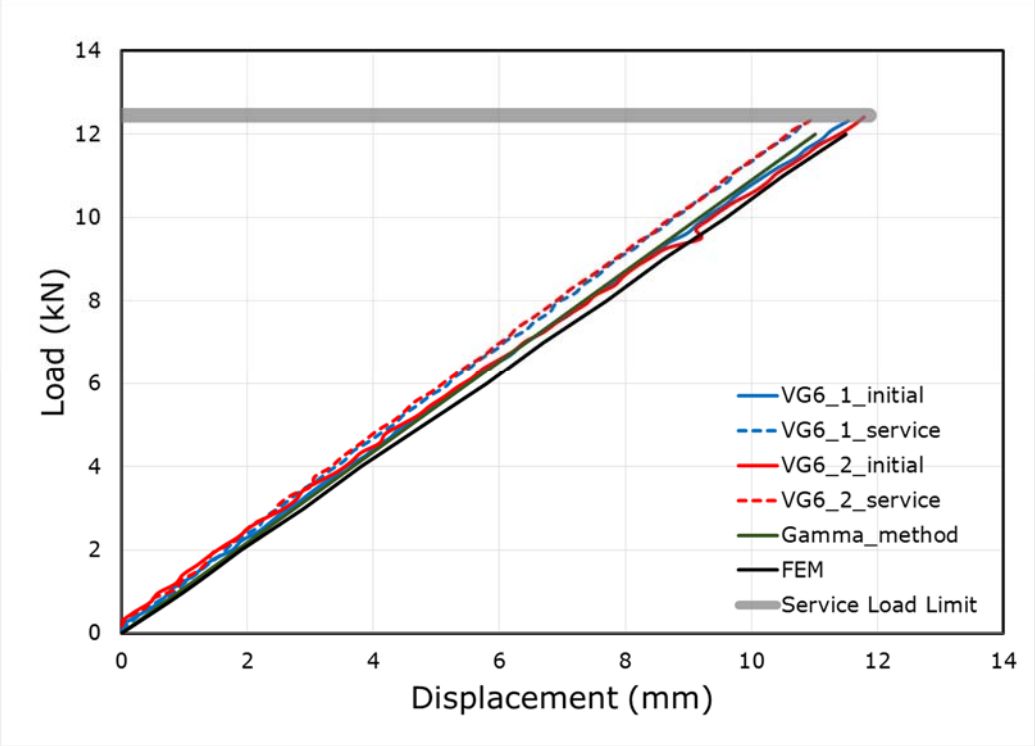

Figure 38: Load vs. Displacement of Series 2 up to Service Level

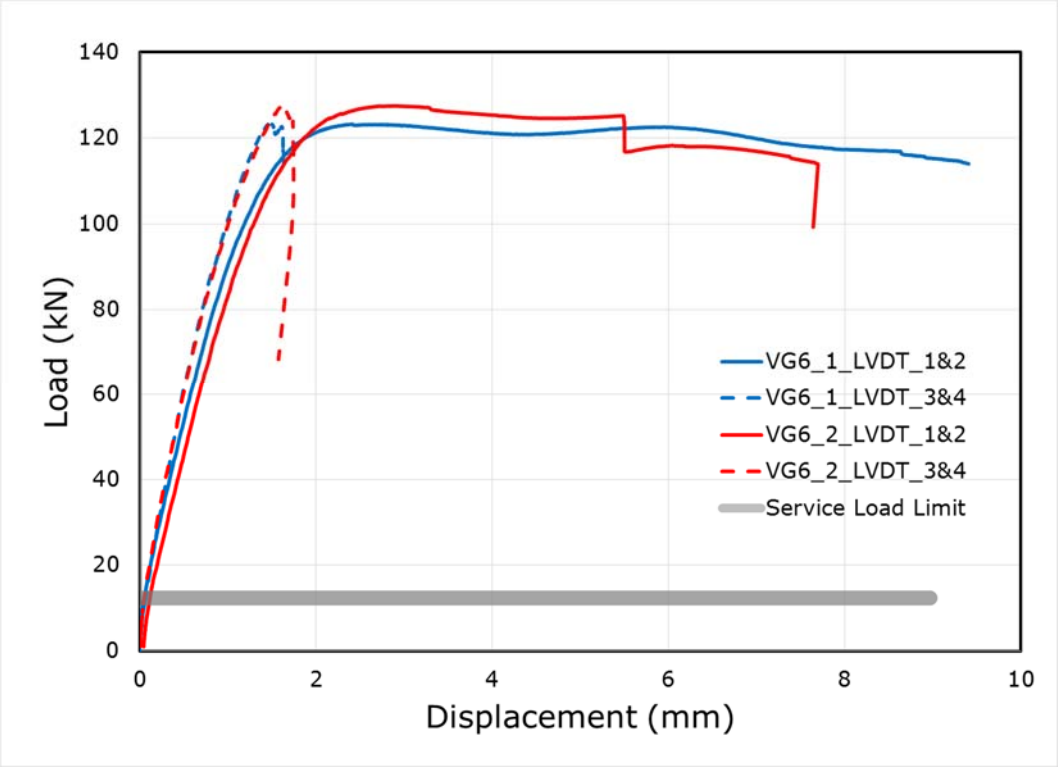

Figure 39: Load vs Shear Slip of of Series 2

Series 3: Screws installed at 30^0 in CLT

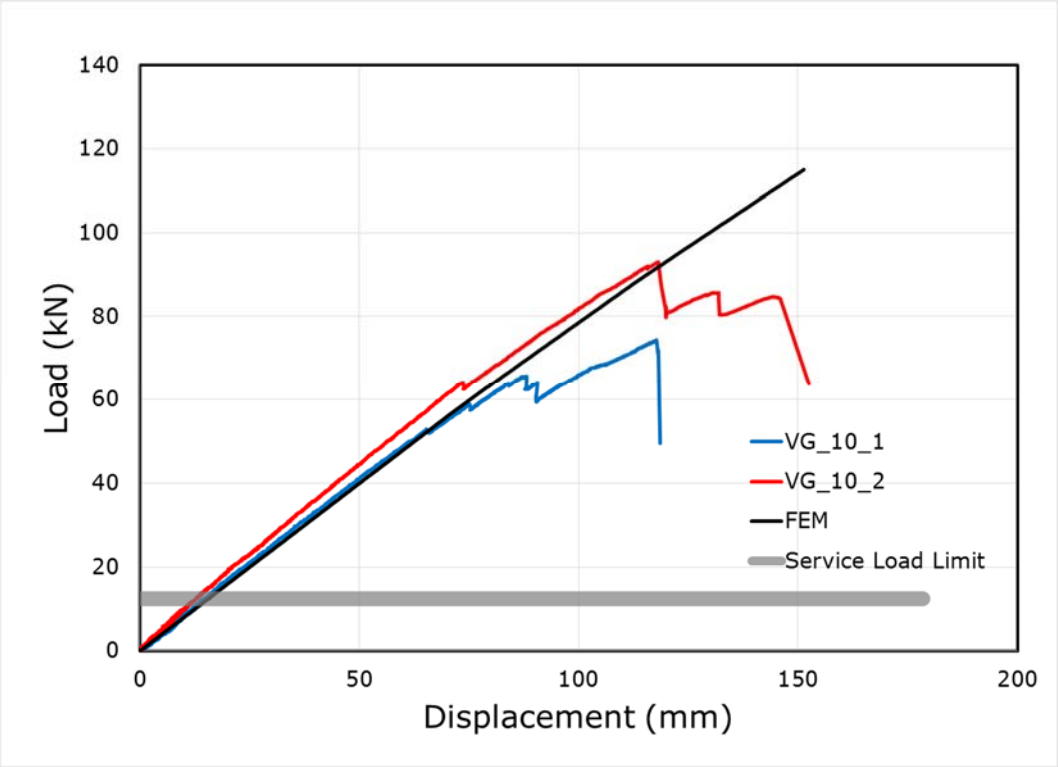

Figure 40: Load vs. Displacement of series 3

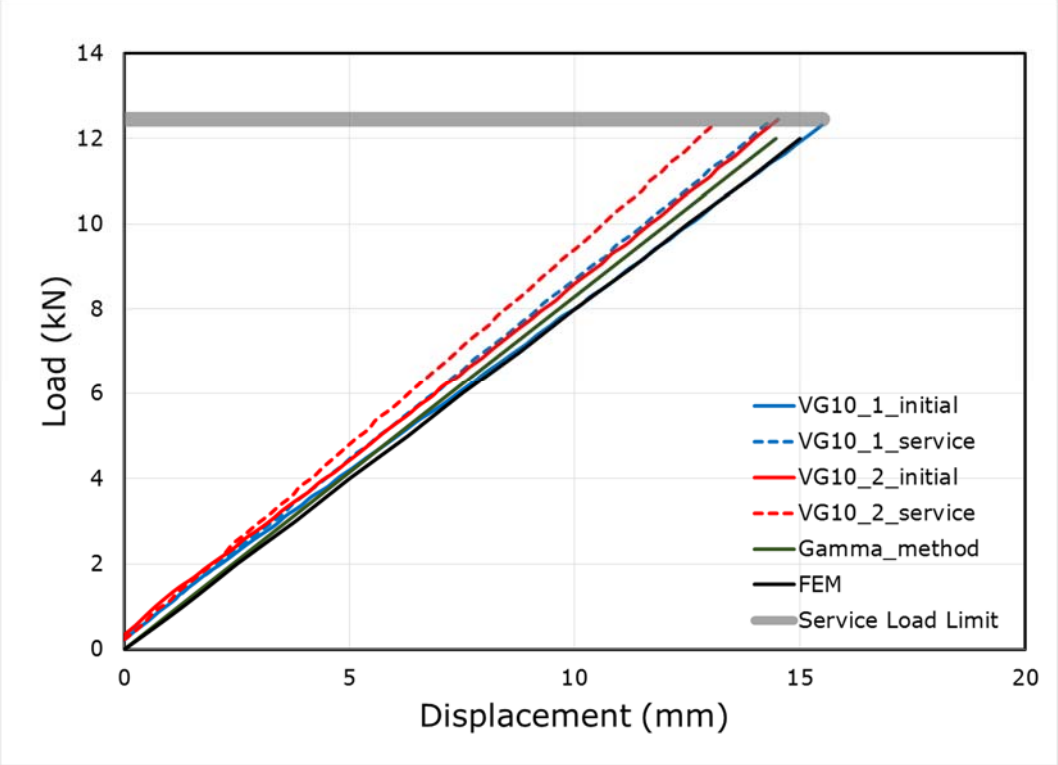

Figure 41: Load vs. Displacement of series 3 up to Service Level

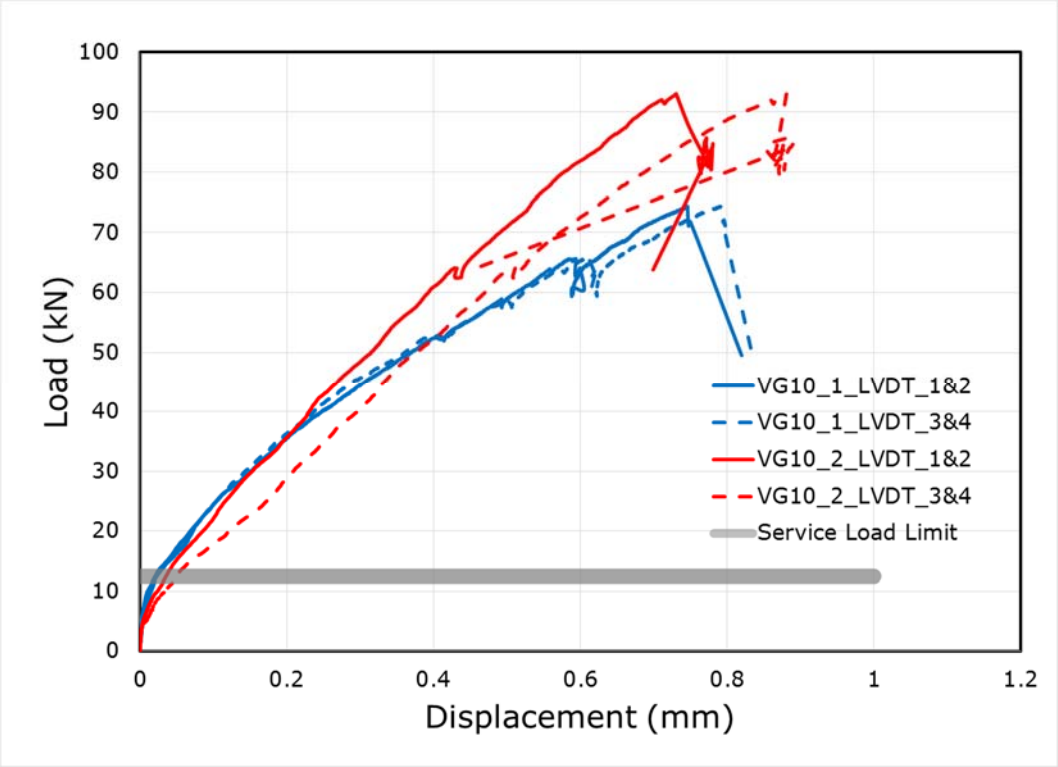

Figure 42: Load vs Shear Slip of series 3

Series 4: Screws installed at 45^0 pairs through 25mm insulation in LSL

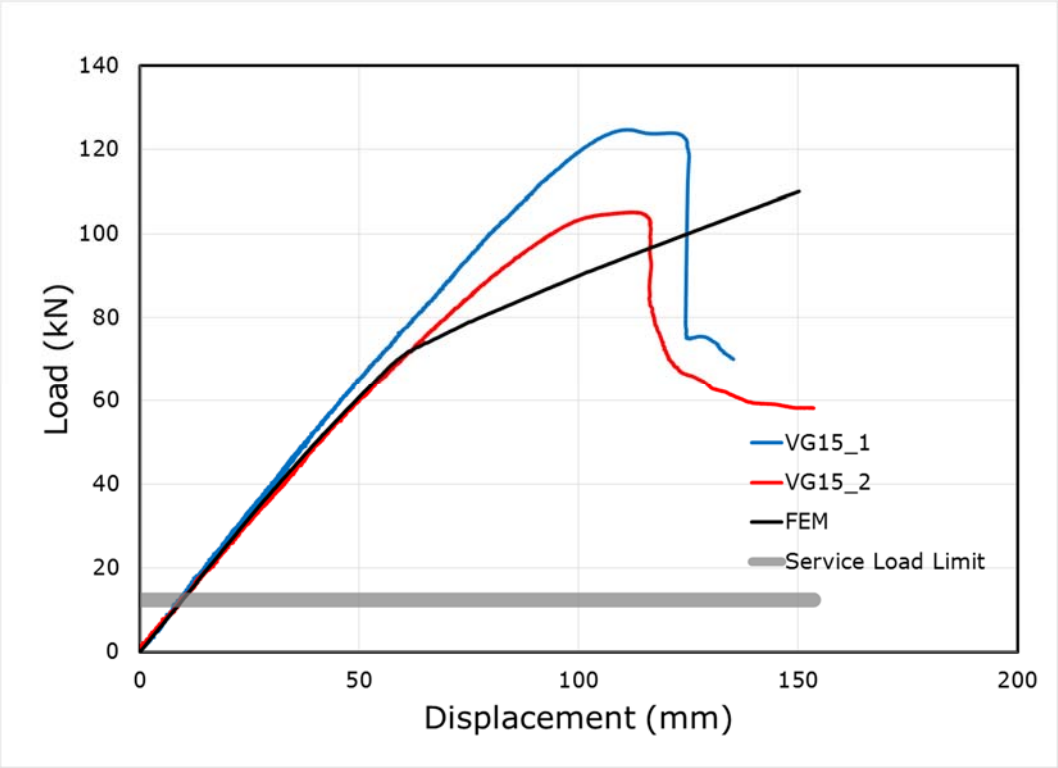

Figure 43: Load vs. Displacement of series 4

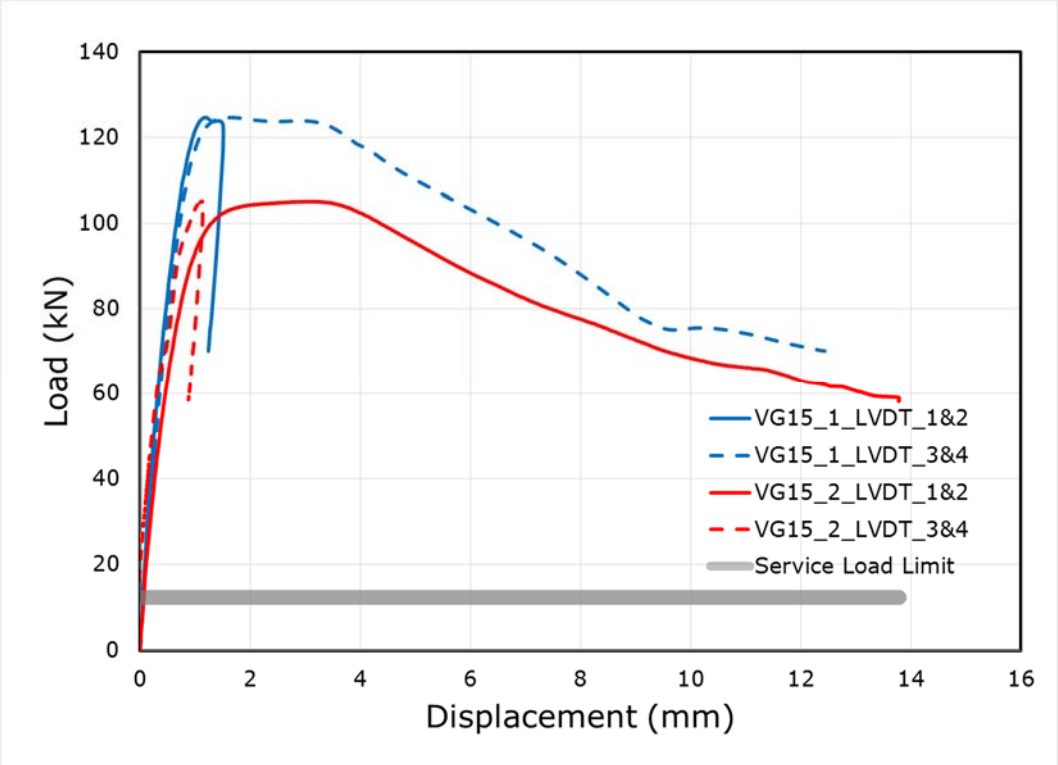

Figure 44: Load vs. Displacement of series 4 up to Service Level

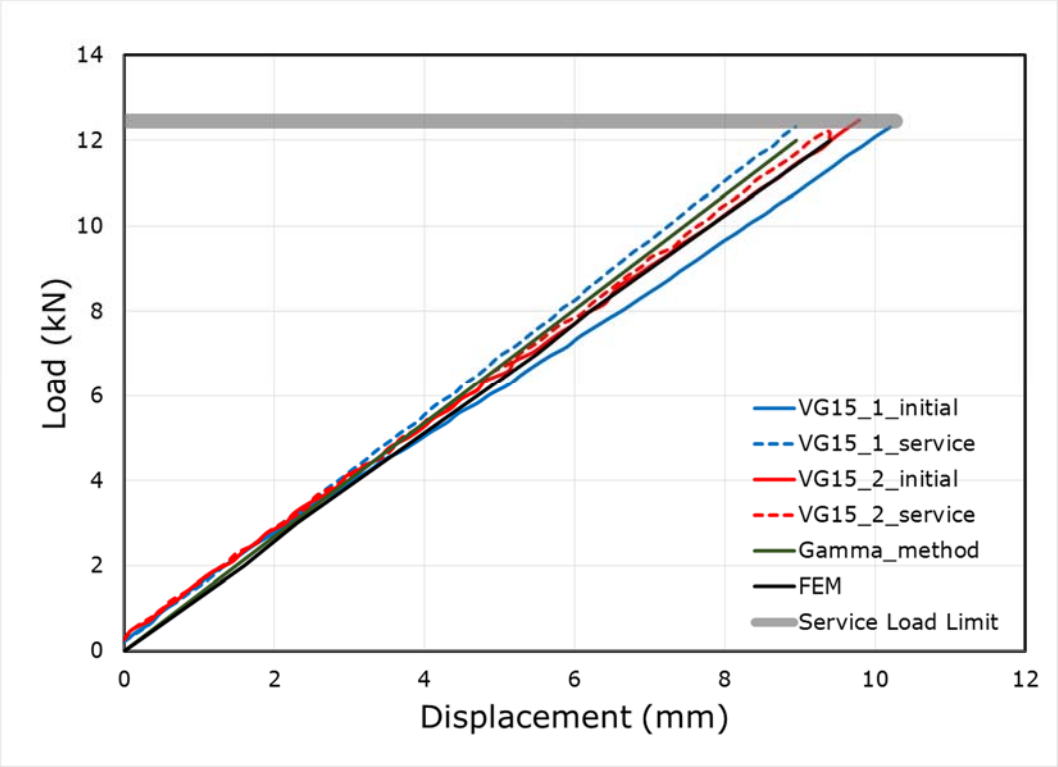

Figure 45: Load vs Shear Slip of series 4

Series 5: Screws installed at 30^0 combined with adhesive layer in LVL

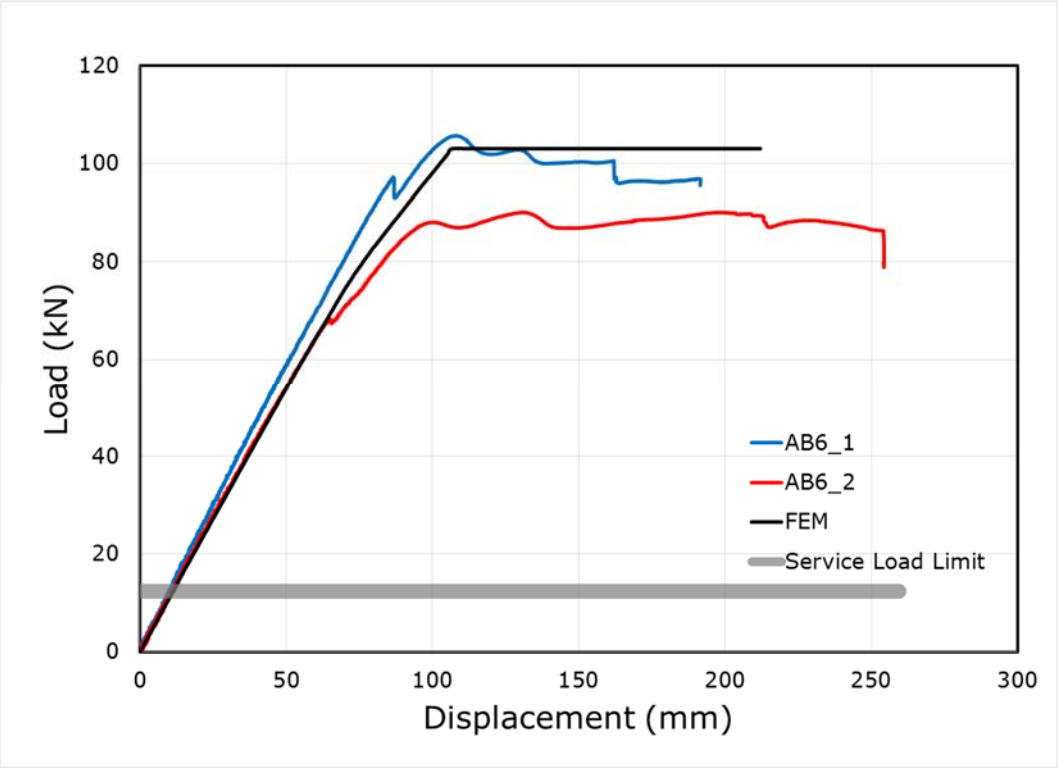

Figure 46: Load vs. Displacement of series 5

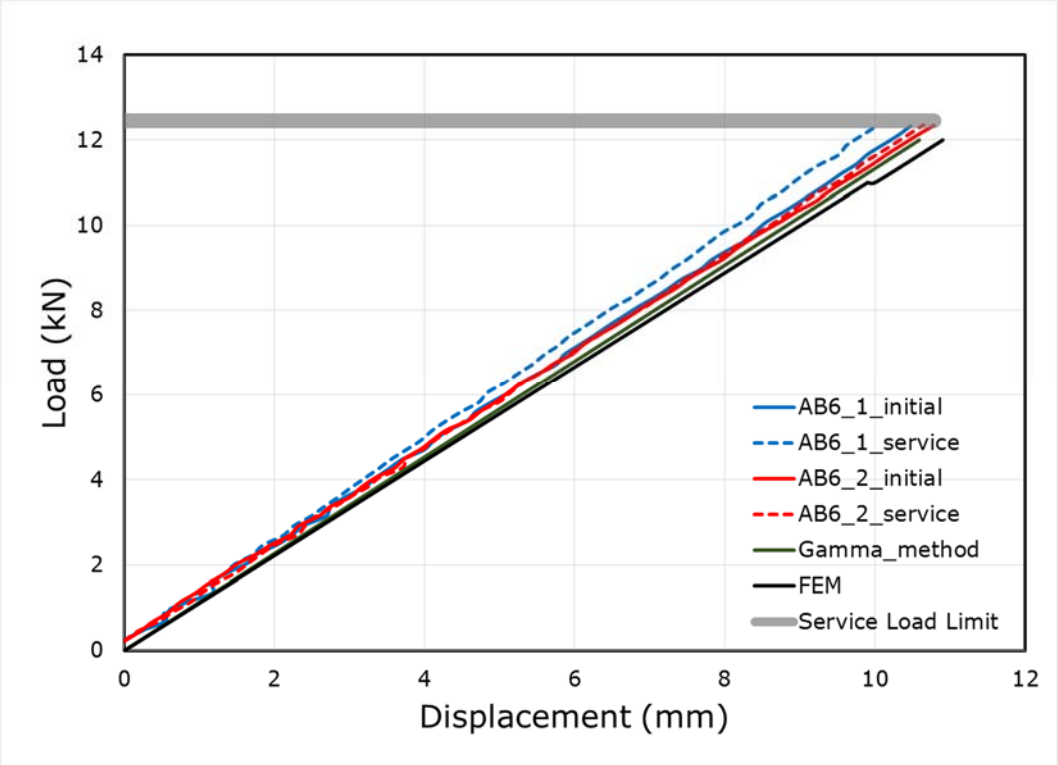

Figure 47: Load vs. Displacement of series 5 up to Service Level

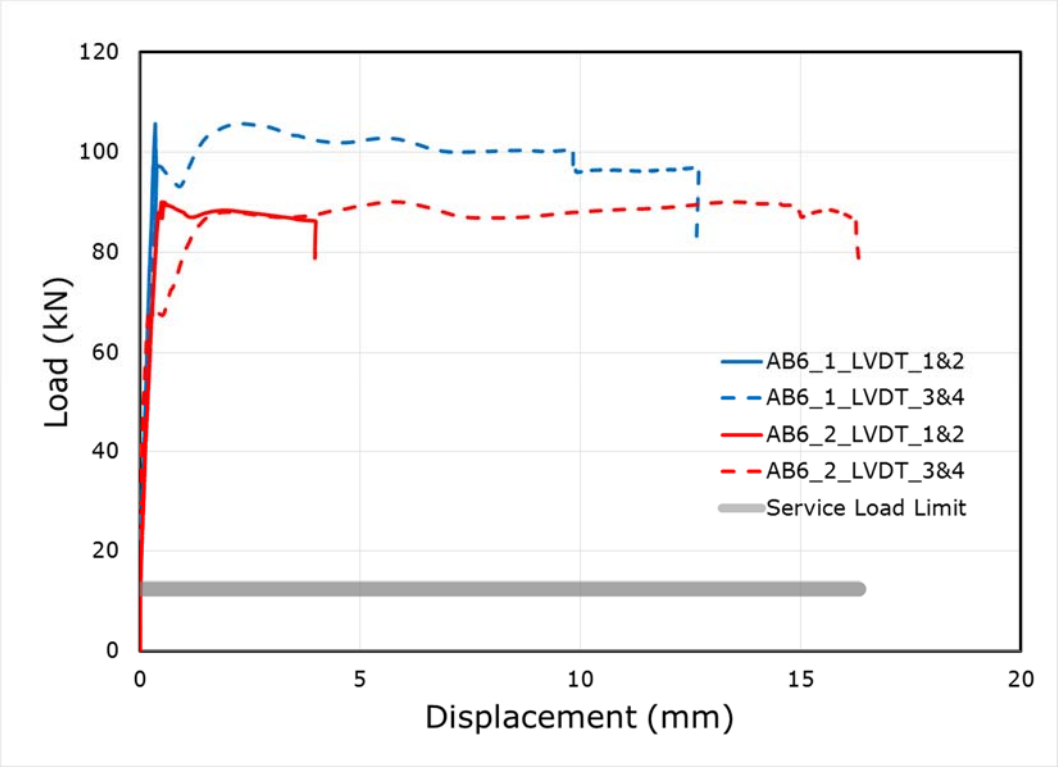

Figure 48: Load vs Shear Slip of series 5

Series 6: HBV mesh installed in LSL

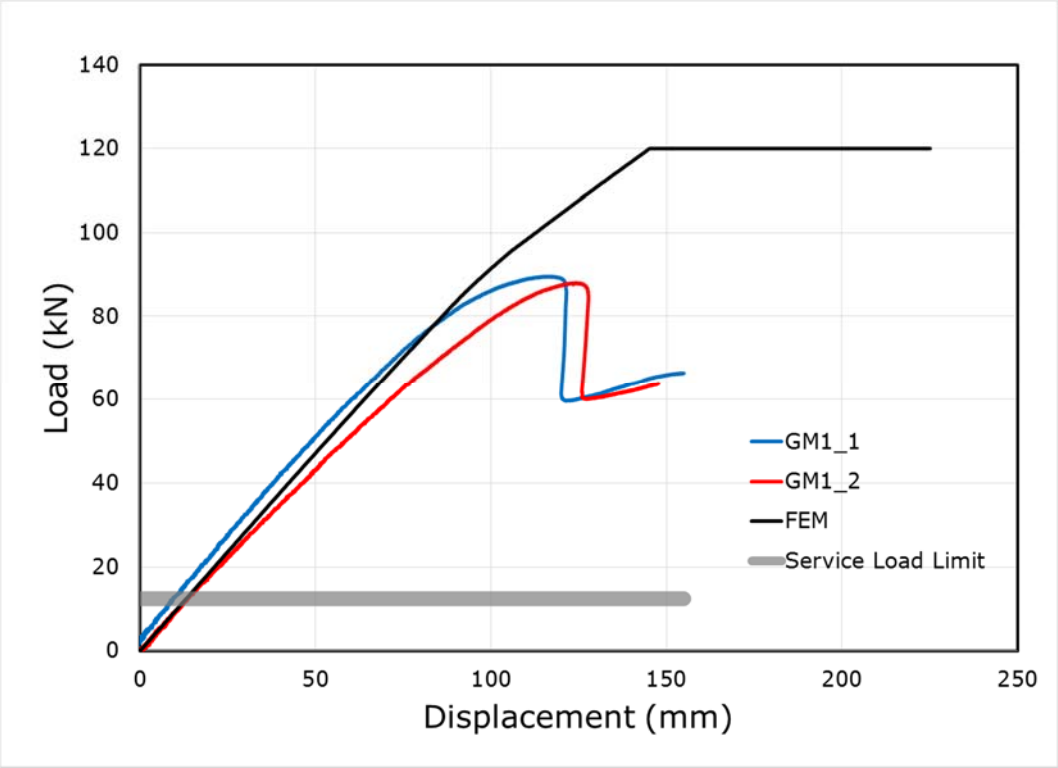

Figure 49: Load vs. Displacement of series 6

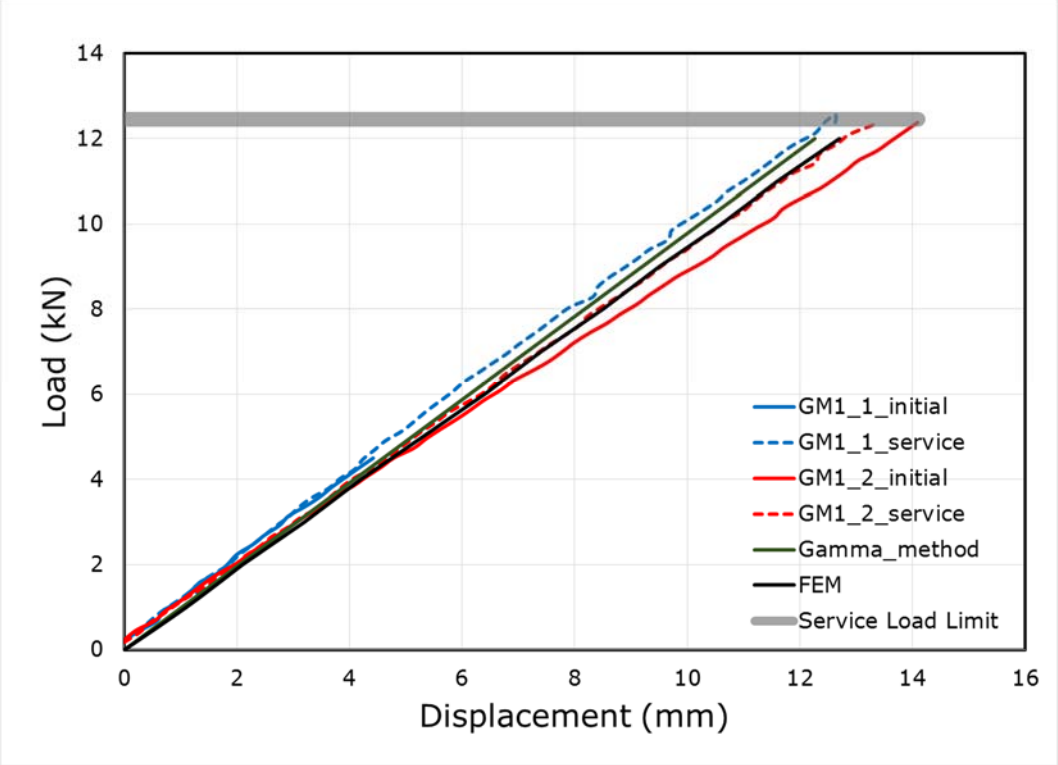

Figure 50: Load vs. Displacement of series 6 up to Service Level

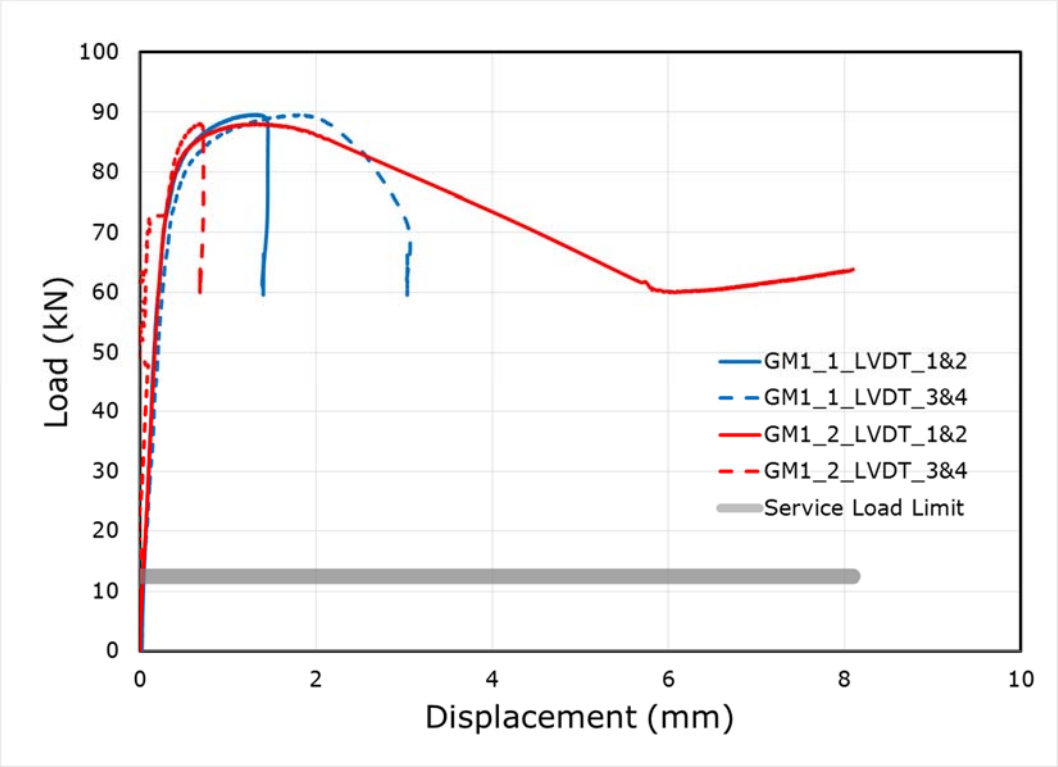

Figure 51: Load vs Shear Slip of series 6

Series 7: HBV mesh installed in LVL

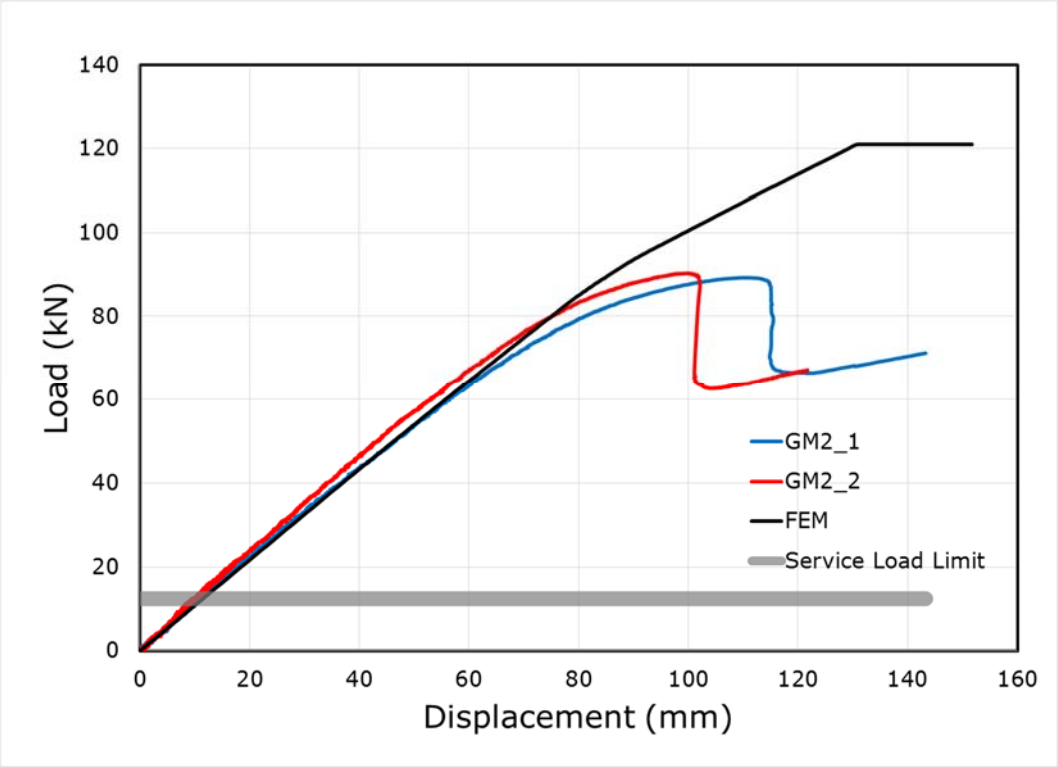

Figure 52: Load vs. Displacement of series 7

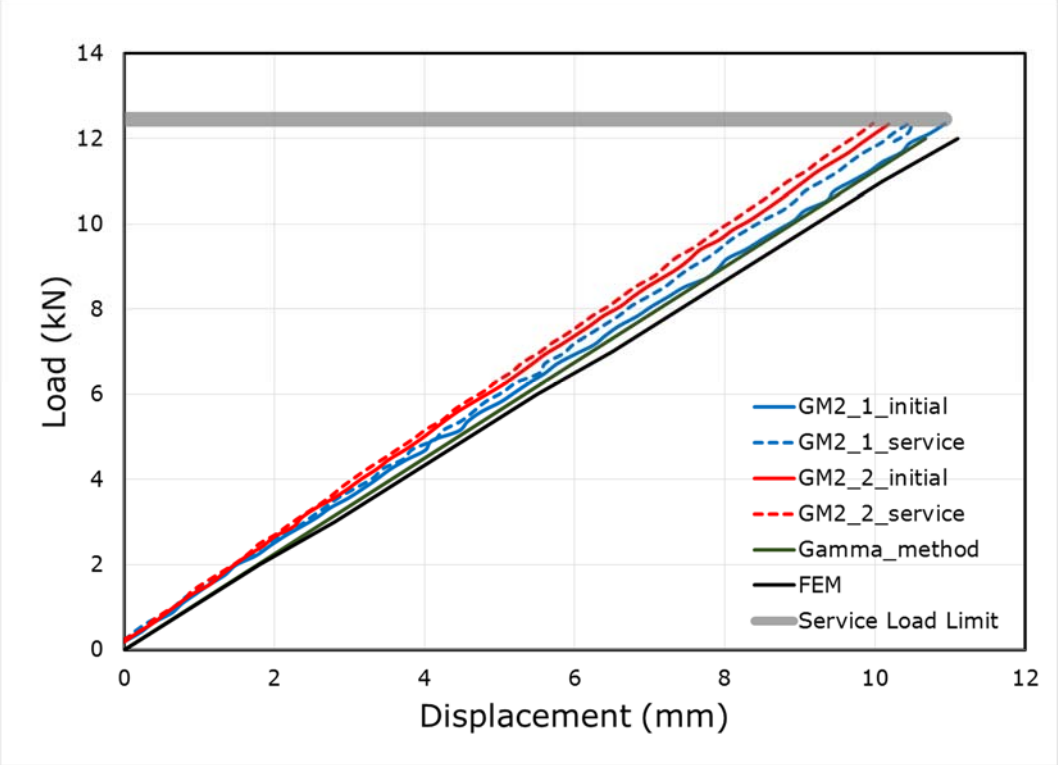

Figure 53: Load vs. Displacement of series 7up to Service Level

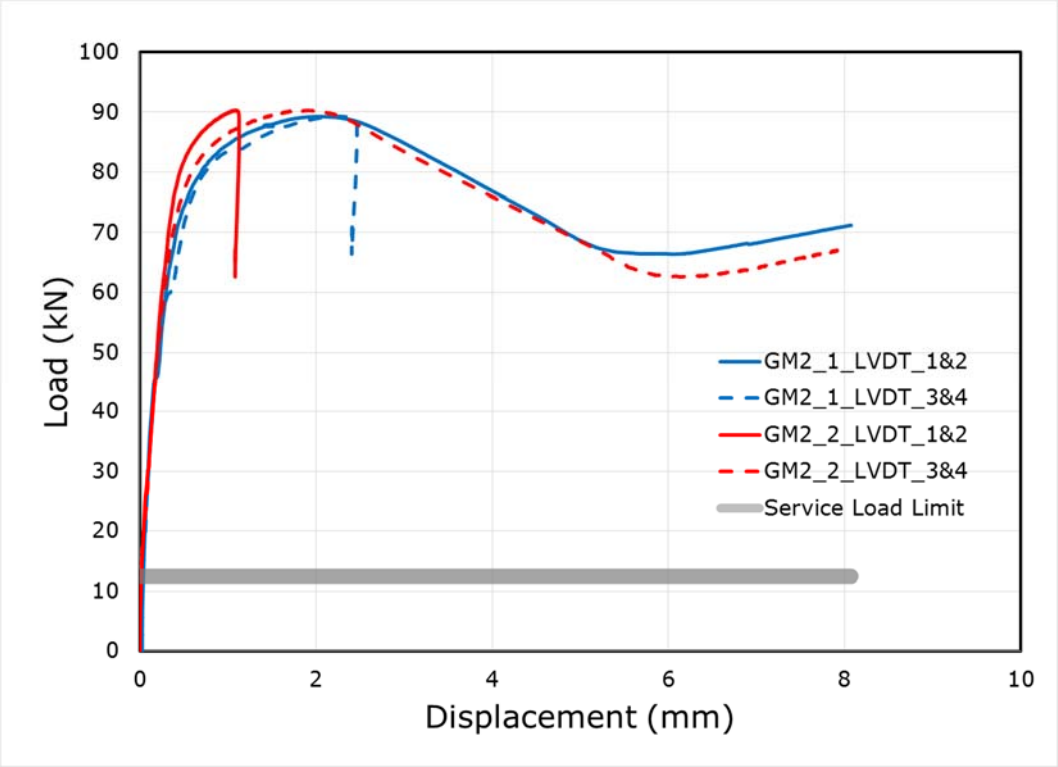

Figure 54: Load vs Shear Slip of series 7

Series 8: HBV mesh installed in CLT

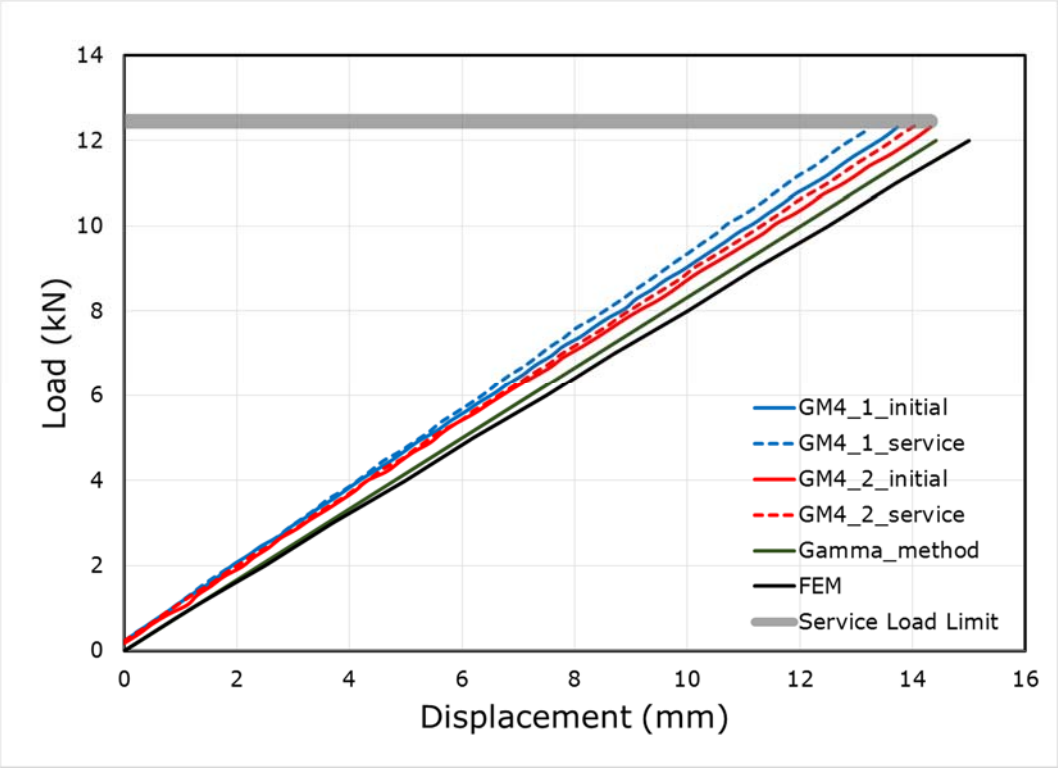

Figure 55: Load vs. Displacement of series 8

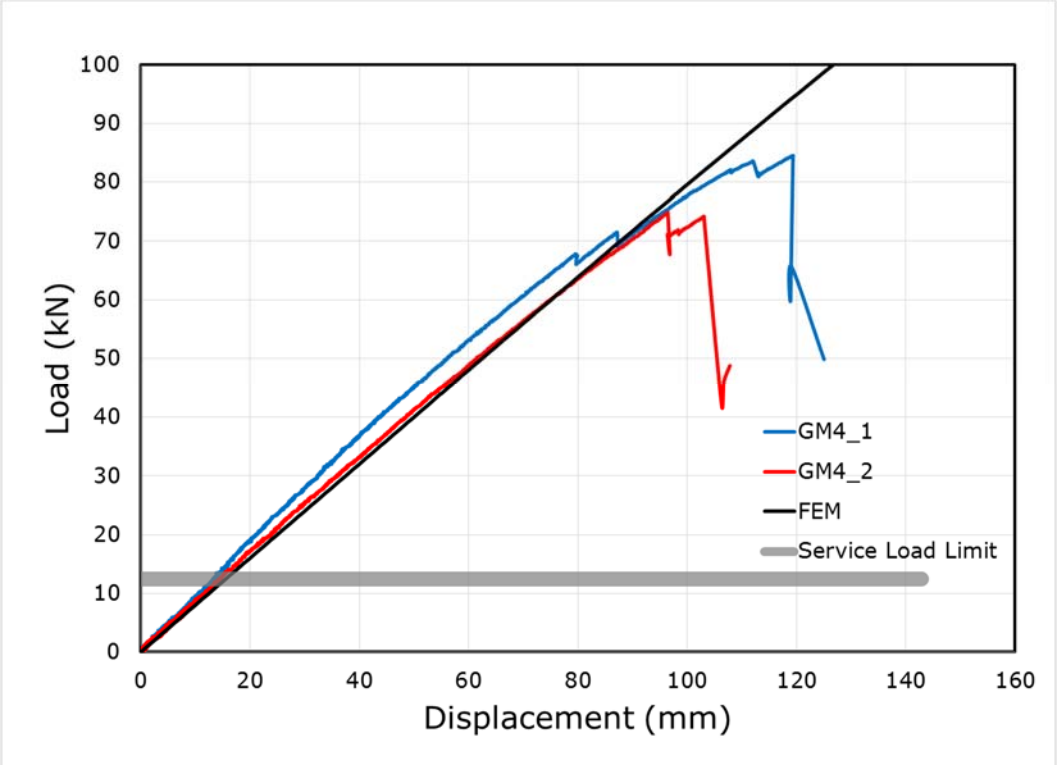

Figure 56: Load vs. Displacement of series 8 up to Service Level

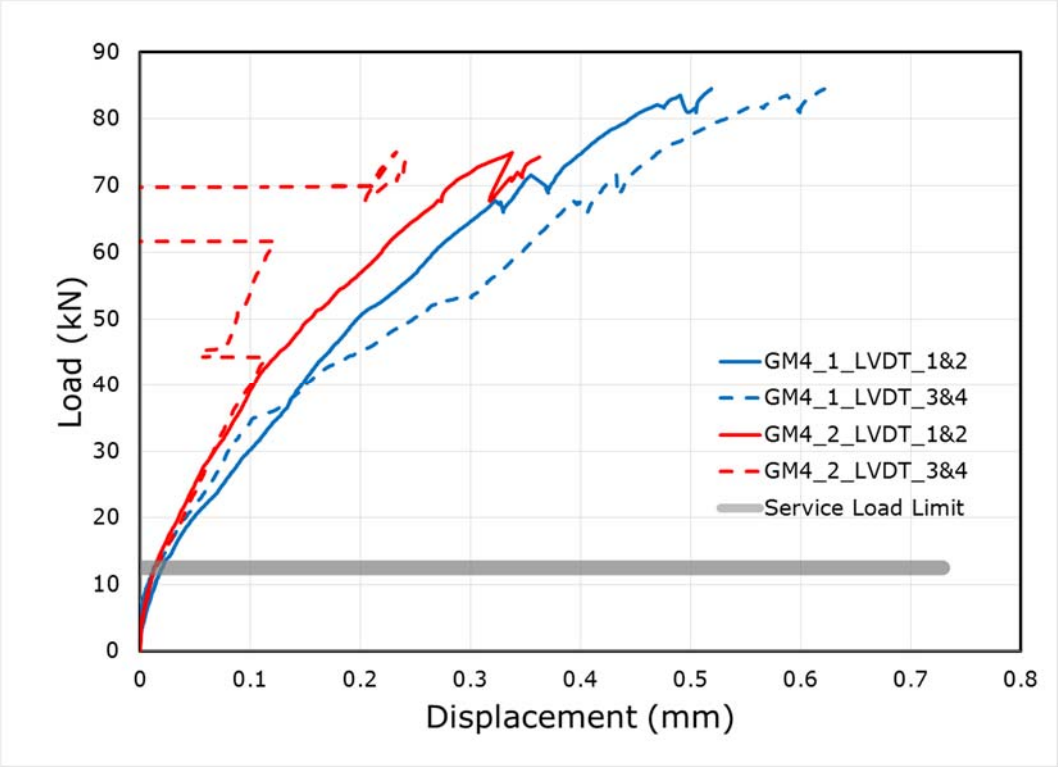

Figure 57: Load vs Shear Slip of series 8

Series 9: HBV mesh installed through 25mm insulation in LVL

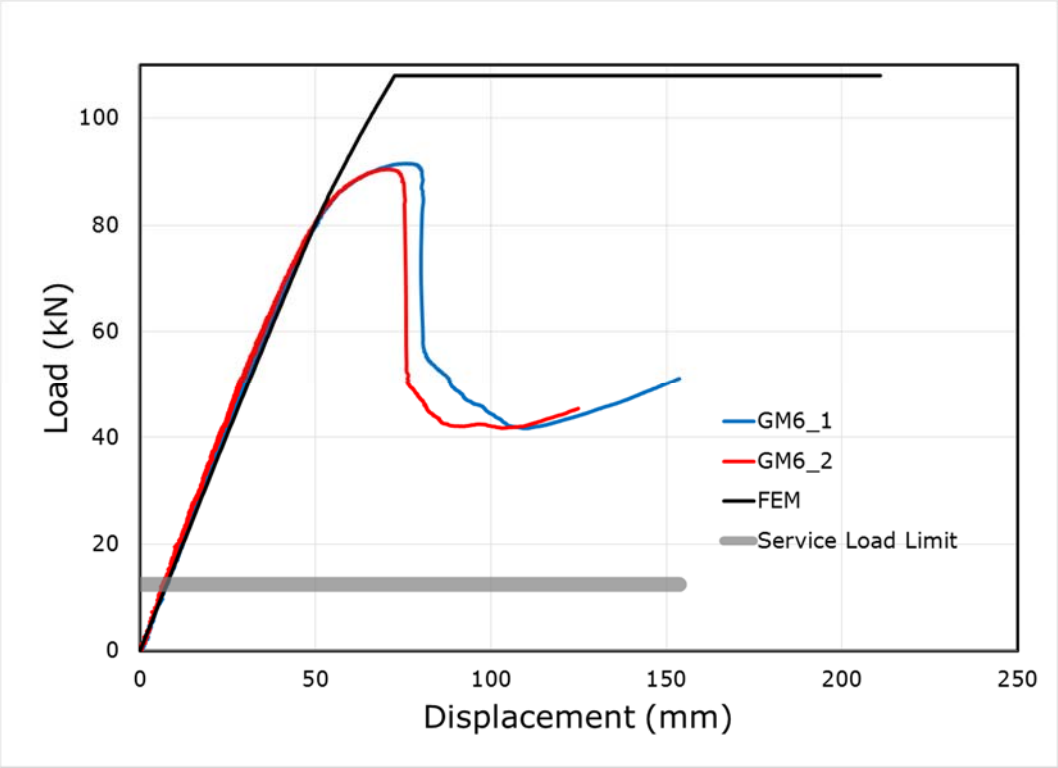

Figure 58: Load vs. Displacement of series 9

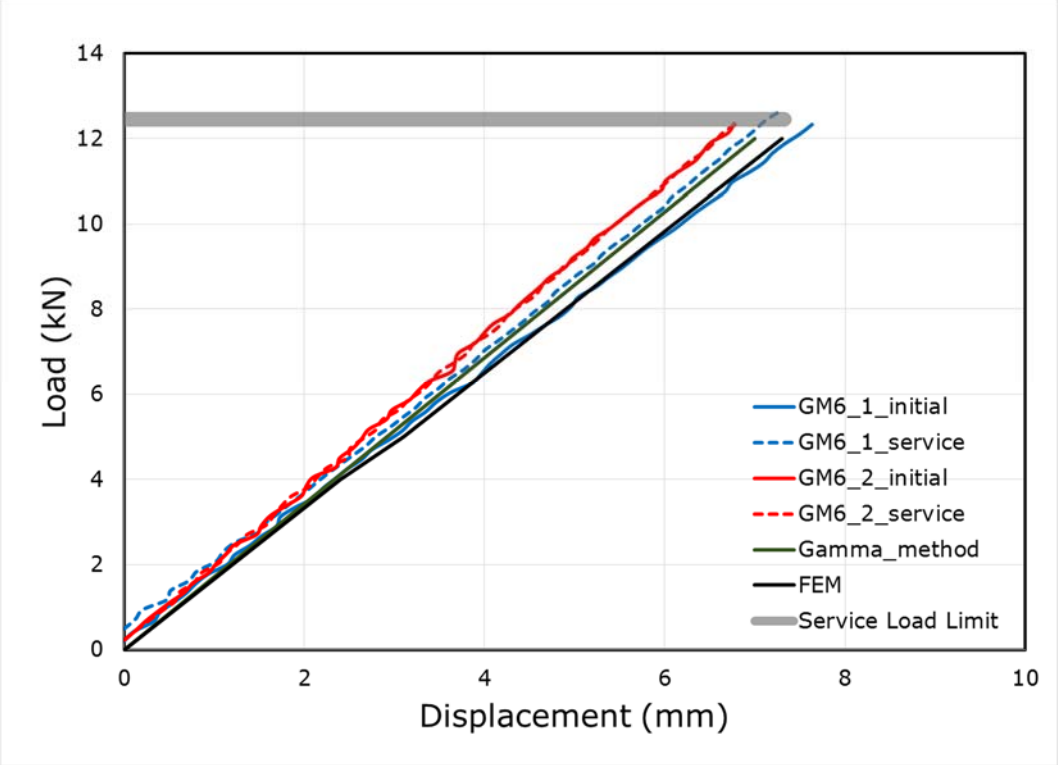

Figure 59: Load vs. Displacement of series 9 up to Service Level

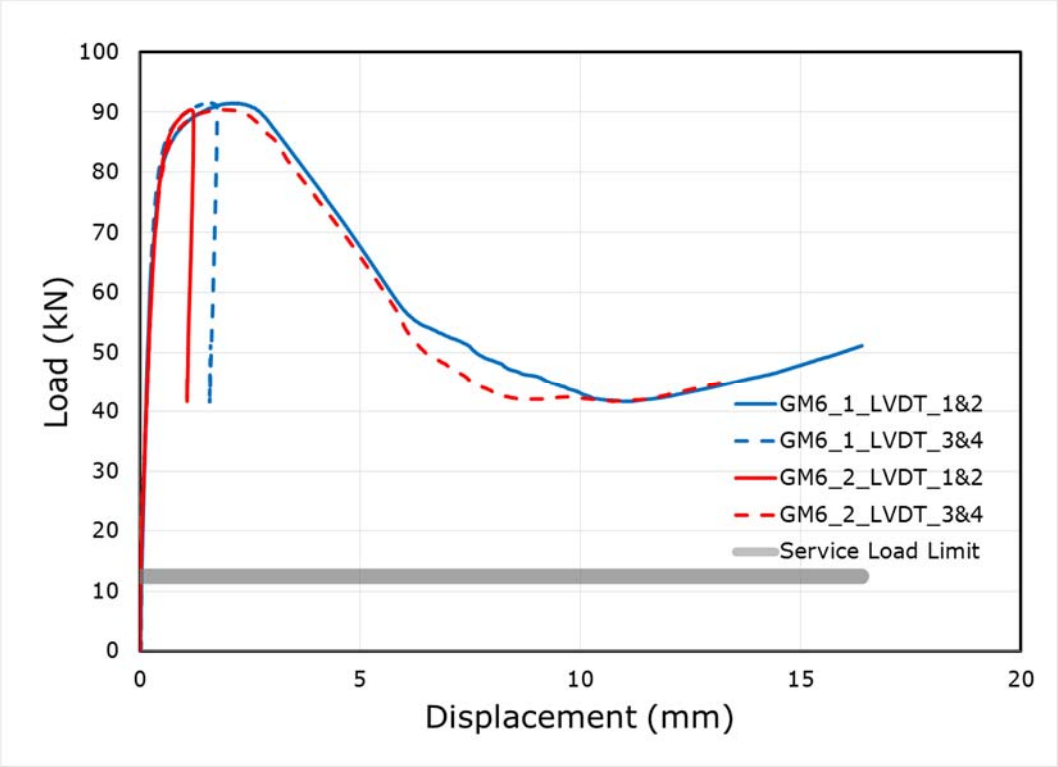

Figure 60: Load vs Shear Slip of series 9

Appendix E: Pictures of failure modes

Concrete crushing and timber tensile failure

Figure 61: Series 1 Panel failing due to concrete crushing and timber tensile fracture

Connector failure followed by brittle panel failure

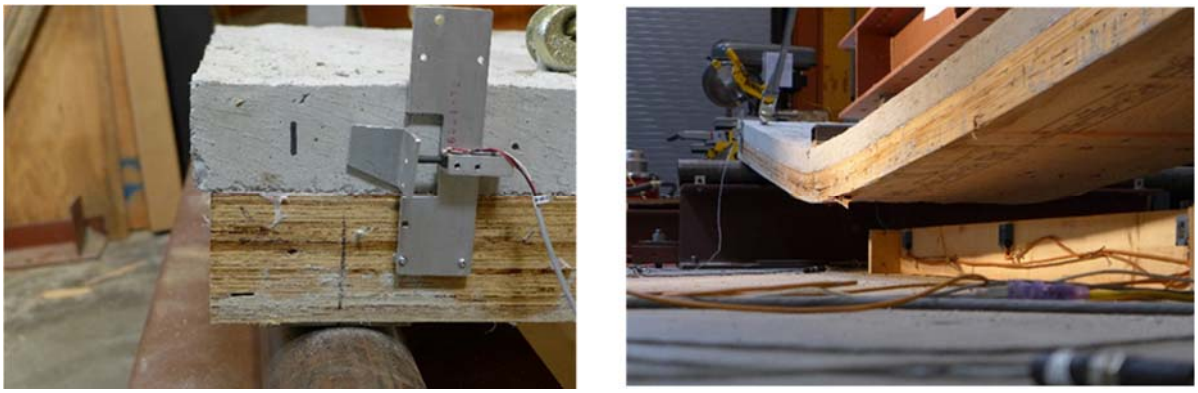

Figure 62: Series 2 panel failing by screw withdrawal followed by tensile failure of timber

Brittle tensile failure of timber

Figure 63: Series 3 panel exhibiting tensile failure prior to connector yielding or concrete crushing

Ductile screw withdrawal failure

Figure 64: Series 4 panel failing by screw withdrawal through 25mm rigid insulation

Ductile connector yielding failure

Figure 65: Series 7 panel with HBV connector prior to (left) and after yielding (right)

Bond failure, screw withdrawal and timber tensile failure

Figure 66: Series 5 panel failures (a) initial failure of adhesive bond line followed by (b) screw withdrawal failure and finally (c)(d) timber tensile failure

Ductile connector yielding failure through rigid insulation

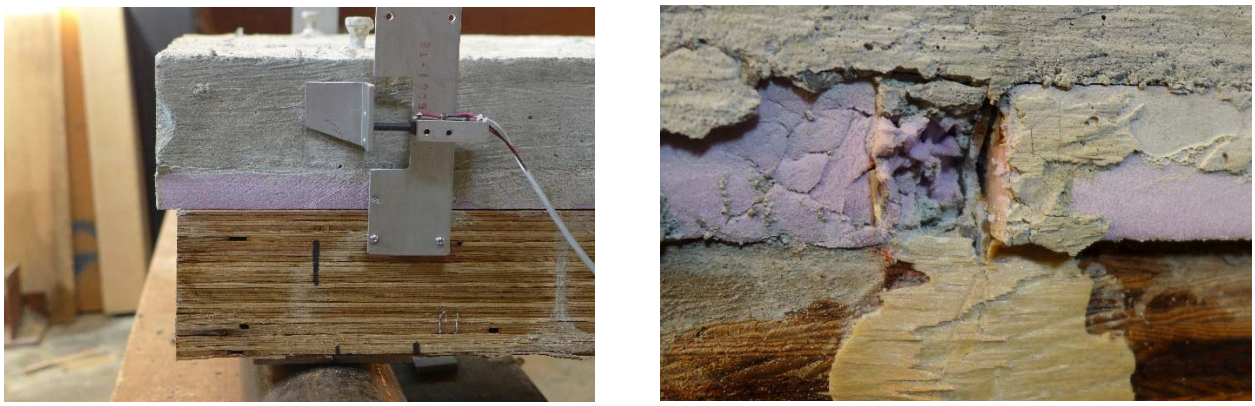

Figure 67: Series 9 panel with HBV connector yielding through 25mm rigid insulation